MN ON CE MODIFIED AL_2O_3 OXYGEN CARRIERS FOR LIQUID FUEL BASED CHEMICAL LOOPING COMBUSTION

BY

ABDULHADI ABDULLAH ALZAHRANI

A Thesis Presented to the

DEANSHIP OF GRADUATE STUDIES

KING FAHD UNIVERSITY OF PETROLEUM & MINERALS

DHAHRAN, SAUDI ARABIA

In Partial Fulfillment of the
Requirements for the Degree of

MASTER OF SCIENCE

In

CHEMICAL ENGINEERING

APRIL 2016

KING FAHD UNIVERSITY OF PETROLEUM & MINERALS
DHAHRAN- 31261, SAUDI ARABIA
DEANSHIP OF GRADUATE STUDIES

This thesis, written by Abdulhadi Al-Zahrani under the direction his thesis advisor and approved by his thesis committee, has been presented and accepted by the Dean of Graduate Studies, in partial fulfillment of the requirements for the degree of **MASTER OF SCIENCE IN CHEMICAL ENGINEERING.**

Mozzhar Hossain
Dr. M. Mozahar Hossain
(Advisor)

Dr. Mohammed Ba-Shammakh
Department Chairman

Shaikh Abdur Razzak
Dr. Abdur Razzak Shaikh
(Co-Advisor)

Dr. Salam A. Zummo
Dean of Graduate Studies

R.H.
Dr. Housam Binous
(Member)

26 April 2016
Date

OKI MURAZA
Dr. Oki Muraza
(Member)

Dr. Zuhair Malibari
(Membe

Abdulhadi Al-Zahrani

2016

ACKNOWLEDGMENTS

I would like to acknowledge my Thesis advisor Dr. Mozahar Hossain and my co-advisor Dr. Shaikh Abdur Razzak for their support and encouragement. Also, I would like acknowledge my Thesis committee members: Dr. Hosam Binous, Dr. Oki Muraza and Dr. Zuhair Malibari for their valuable comments and suggestions.

Finally, I would like to express my sincere gratitude to my family and friends for their love and support.

TABLE OF CONTENTS

LIST OF TABLES

LIST OF FIGURES

ABSTRACT

Full Name : Abdulhadi Al-Zahrani
Thesis Title : Mn on Ce Modified Al2O3 oxygen carrier for liquid fuel based chemical looping combustion

Major Field : Chemical Engineering

Date of Degree : April 2016

In this study we investigated Ce modified MnO_x/Ce-γAl_2O_3 oxygen carriers for liquid fuel based chemical looping combustion. The support γAl_2O_3 was modified with 1% Ce to provide thermal stability of the material and to minimize the metal support interaction. On the other hand, MnO_x was used as the actual oxygen carrier. Both Ce and Mn were loaded on the support by an incipient wetness technique using a successive metal loading. In order to ensure the desired characteristics, the prepared oxygen carriers were characterized using various physicochemical techniques such as XRF, nitrogen adsorption, TGA, XRD, SEM, TPR, TPO and TPD. TGA and XRD analysis show that Ce modification improves the thermal stability of γAl_2O_3 and hinders the formation of difficult reducing manganese aluminate. TPR result shows excellent reduction and re-oxidation performances of manganese oxide supported on the Ce modified γAl_2O_3. Almost 83% of the loaded MnO_x has been reduced during the TPR, which also remained consistent over repeated TPR/TPO cycles. The oxygen carriers were further evaluated in a fluidized CREC Riser Simulator using hexane as a liquid fuel at fluidized conditions as expected in an actual CLC process. Under the studied reaction conditions, CO_2 is the main combustion products, which is highly desirable to achieve complete fuel

combustion. Over 90 % hexane combustion was achieved at 575 °C. The solid state kinetics of the fuel-oxygen carrier reaction was also conducted using both the TPR and the CREC Riser Simulator data. A nucleation and nuclei growth model describes the solid-state reduction kinetics of the prepared oxygen carrier adequately. The estimated activated energy of MnO_x/Ce-γAl_2O_3 reduction were found to be 27 kJ/mole and 59 kJ/mole using hydrogen and hexane, respectively.

ملخص الرسالة

الاسم الكامل:عبدالهادي عبدالله حسن العُمري الزهراني

عنوان الرسالة: اضافة السيريوم الى مركبات أوكسيد المنجنيز المثبت على أوكسيد الالمنيوم كناقلات للأوكسجين في احتراق الوقود السائل.

التخصص: هندسة كيميائية

تاريخ الدرجة العلمية: أبريل 2016

في هذه الدراسة تم دراسة معالجة ناقلات الأكسجين MnOx / Ce-γAl2O3 لاحتراق الوقود السائل. تم تعديل γAl2O3 مع 1٪ Ce لتوفير الاستقرار الحراري للمواد والتقليل من التفاعل بين الداعم والمعدن الفعال. من ناحية أخرى، كان يستخدم MnOx باعتبارها الناقل الأكسجين الفعلي. من أجل ضمان الخصائص المرغوبة، تم تحليل العينات- المحضرة بتقنية التحميل- باستخدام مختلف التقنيات الفيزيائية مثل XRF، امتصاص النيتروجين، TGA، حيود الأشعة السينية، SEM، TPR، TPO. TGA وتحليل حيود الأشعة السينية تظهر أن اضافة السيريوم تحسن الاستقرار الحراري للγAl2O3 ويعيق تشكيل ألومينات المنغنيز الذي تم تأكيده من اختبار XRD. كما تظهر النتائج أن 83% من المنجنيز تم اختزاله في العينات المعدلة بالسيريوم. أيضا, أظهرت العينات أداء مستقرا فيما يتعلق بنسبة الاختزال للمنجنيز في عمليات الاختزال المتتالية. أيضا , من خلال نموذج رياضي , تم حساب طاقة التفعيل لتكون 26.9 kJ/mol للاختزال مع غاز الهيروجين في اختبار TPR مقارنة بـ 59.2 kJ/mol مع الهيكسين. أخيرا, أظهرت العينات المعدلة كفاءة عالية في مفاعل Riser باستخدام الهيكسين كوقود سائل.

CHAPTER 1

INTRODUCTION

1.1 Introduction

Studies shows that over the second half of the twentieth century the surface temperatures of the earth have been rising dramatically (Figure 1.1)(Edenhofer et al., 2011). This increase in the earth temperature, commonly known as a global warming, is attributed mainly to the emissions of greenhouses gases. The majority of the greenhouse gases emission is contributed by water vapor (H_2O), carbon dioxide (CO_2) and methane (CH_4). The most abundant gas among these greenhouse gases is CO_2 which result at most affected by human activity and industry (Hossain & de Lasa, 2008). The most significant source of emitted CO_2 into the atmosphere is the combustion of fossil fuels. The use of coal alone accounted for 43% in 2010 (Yu, 2013). According to US Department of Commerce, 2014, the atmospheric concentration of CO_2 in 2010 was 390 ppm compared with 280 ppm in 1750 in the era of pre-industrial(Figure 1.2).

As a result of these concerns of global warming, it is necessary to find ways to minimize the greenhouse gas emission. Therefore, developed countries have ratified the Paris Agreement in a bid to an international effort to reduce carbon dioxide emissions. As a result of the fact that fossil fuels is the main source of energy now and in the near future, it was imperative to find appropriate solutions to prevent emissions from this fuel.

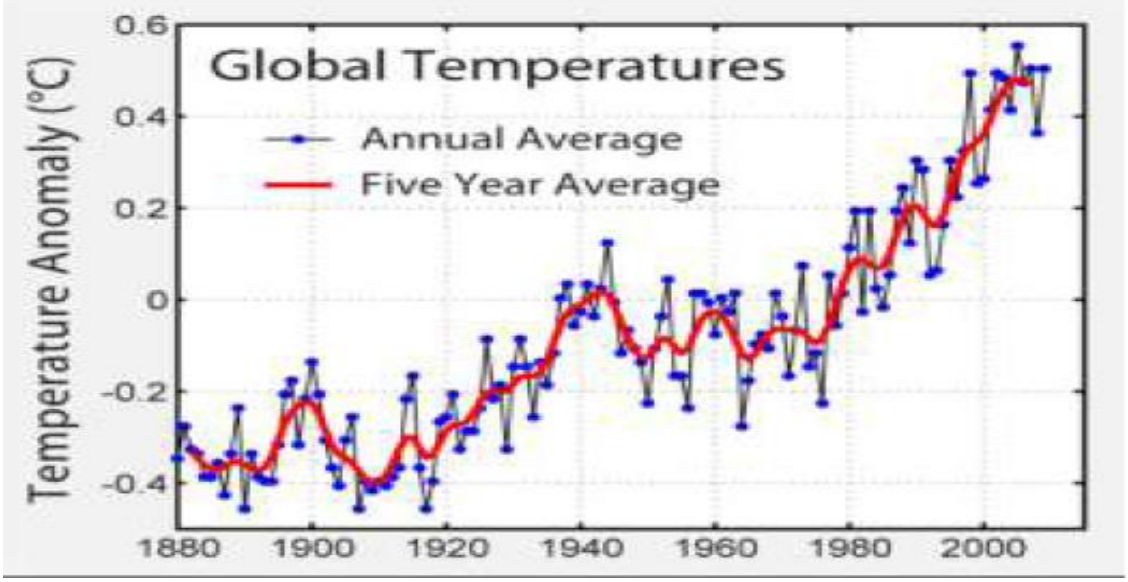

Figure 1.1 Surface temperature global mean difference relative to the 1961–1990 average(Hansen et al. 2006).

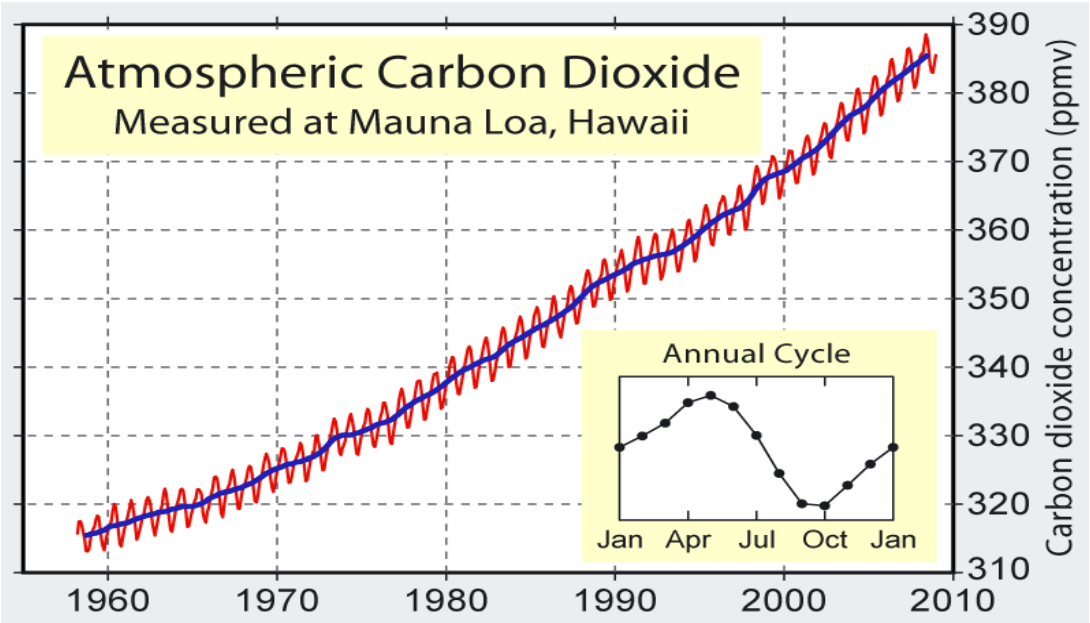

Figure 1.2 CO2 concentrations measured at Mauna Loa Observatory (US Department of Commerce, 2014).

One of these methods was Carbon Capture and Storage (CCS). The purpose of CCS

technology is to produce a concentrated stream of CO_2 from industrial and energy-related sources, transport it to a suitable storage location, and then store it away from the atmosphere for a long period of time.

1.2 Carbon Dioxide Capture

Three main technologies for CO_2 capture from power production have been evaluated: post-combustion, pre-combustion, and oxy-fuel combustion. In post- combustion, CO_2 is captured from the flue gases produced after the combustion of the fuel. Different processes have been used for the CO_2 capture. These processes include: absorption, adsorption, and membrane or cryogenic processes (Mathias, Reddy, Smith, & Afshar, 2013). However, the concentration of CO_2 in the flue gas for post –combustion processes are typically lower than 15%, which make the driving force for CO_2 capture low and the costs are high. As an example, 30% of energy is required for capturing CO_2 using monoethanolamine (MEA) which will cause to 80% increase in the cost of electricity ("US Department of Energy, Carbon Dioxide Capture and Storage," n.d.)

In pre-combustion capture, also known as IGCC (Integrated Gasification Combined Cycle), the fuel is first gasified with oxygen to produce synthesis gas (Padurean, Cormos, & Agachi, 2012). This gas is then chemically converted into separate streams of carbon dioxide and hydrogen in the so-called water shift reaction ($CO+H_2O \leftrightarrow CO_2+H_2$) converting CO into CO_2 and generating high concentrations of H_2. The CO_2 is then separated using similar methods to those used in post-combustion processing. However, CO_2 capture by pre-combustion processing is expensive. For example, the energy penalty for pre-combustion CO_2 capture was calculated to be 18 %-19 (Jenni, Baker, & Nemet, 2013).

Oxy-fuel combustion involves the burning of a fossil fuel energy source in the presence of pure oxygen and produces flue gas containing primarily CO_2 and water vapor. Water vapor is very easy to condense, resulting in a pure CO_2 stream which is ready to capture. However, an air separation unit is a high-energy consuming process (Jones, Bhattacharyya, Turton, & Zitney, 2011).

These methods required energy penalty which results in a decrease in the overall efficiency. Therefore, new ways to reduce CO_2 emissions from combustion of fossil fuels have to be developed. A new technology that gained attention and showed a fabulous potential for CO_2 capture is Chemical Looping Combustion.

1.3. Chemical Looping Combustion

Chemical looping combustion (CLC) consists of oxidation and reduction reactors where metal oxide particles are being circulating through these two reactors. The metal oxide particles are oxidized with air in an air reactor (oxidation reactor) and the oxidized metal oxide particles are reduced by fuel in a fuel reactor (reduction reactor) as shown in Figure 1.3.

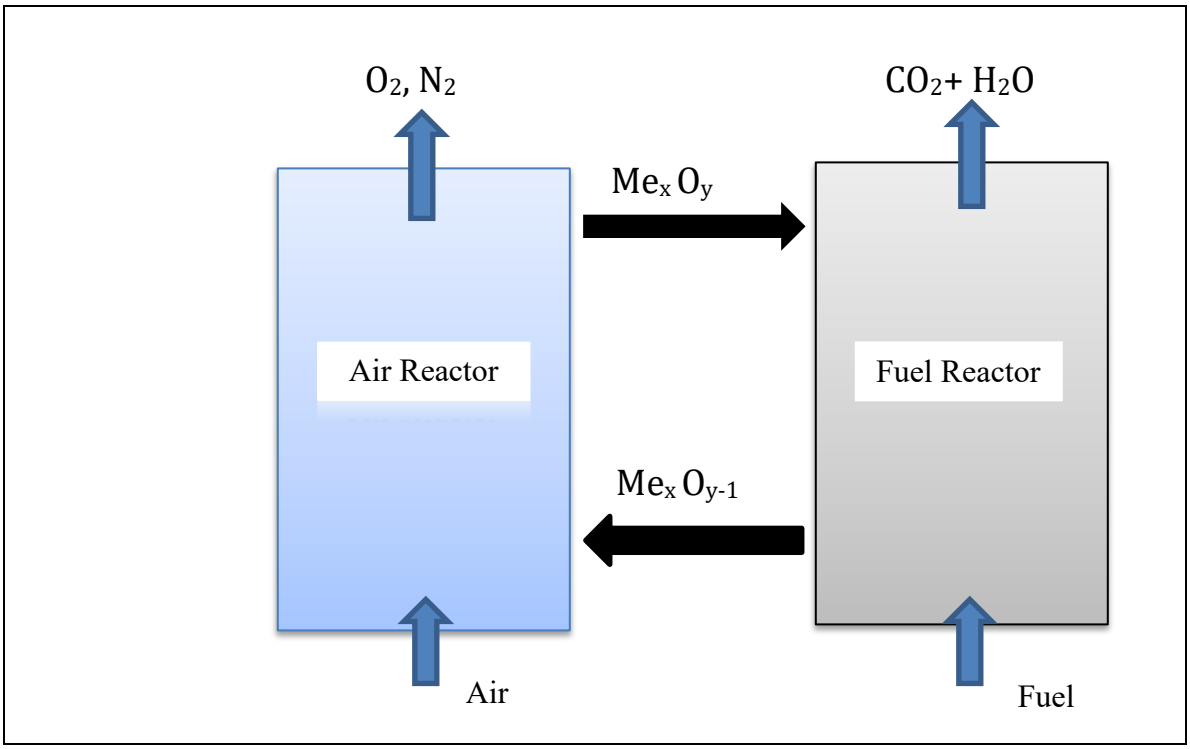

Figure 1.3 Chemical Looping Combustion (CLC) Diagram

The most important characteristic of CLC that the flue gas resulting from this process is composed of water vapor and carbon dioxide and by condensing the water vapor, pure carbon dioxide stream is maintained, which in turn are ready to be sequestrated. Thus, there is no need for extra unit for CO_2 separation. Also, during this process, there is no direct contact between the air and the fuel, which leads to avoid the NO_x emissions.

In the air Reactor, the reaction occurs between the air flow and the oxygen carrier particles according to this reaction:

$$O_2 + 2\ Me_xO_{y-1} \longleftrightarrow 2\ Me_xO_y$$

where Me_xO_{y-1} is a metal oxide and Me_xO_y represents a reduced form of the metal oxide. This reduced oxide is oxidized in the air reactor through the following reaction:

$$(2n+m)Me_xO_y + C_nH_{2n} \longleftrightarrow (2n+m)\ Me_xO_{y-1} + m\ H_2O + n\ CO_2$$

The reduction step is usually endothermic while the oxidation is exothermic. The heat of the reaction depends on the fuel and on the metal oxide used as oxygen carrier. CLC technology is a suitable choice for power generation because the flue gas from the air reactor is at high temperatures which is the same case for the flue gas from the fuel reactor (Fang, Haibin, & Zengli, 2009). Hence, gas and CO_2 turbines can be both used to increase the efficiency which is recently have been confirmed (Brandvoll & Bolland, 2004).

Fluidized bed reactors among reactors types are mostly used in CLC. This is due to the perfect contact between fluid and solid particles in fluidized bed reactors. Also, fluidized bed reactors are applicable when reactivation of solid materials is needed. These two reasons make the fluidized reactors have advantage over alternative designs (Lyngfelt, Leckner, & Mattisson, 2001).

Oxygen carriers are usually transition metal's oxides (Jerndal, Mattisson, & Lyngfelt, 2006a). Good example of transition metals suitable for CLC are copper, nickel, iron and manganese due to their compatible oxidative/reductive properties. The oxygen carrier should be stable under repeated oxidation/reduction cycles at high temperature, resistant to agglomeration, mechanical resistant to the friction stress associated with high circulation of particles and be environmentally and economically feasible (Cho, Mattisson, & Lyngfelt, 2004; Hossain & de Lasa, 2008; Jerndal, Mattisson, & Lyngfelt, 2006b).

This study considers γ-alumina supported manganese based oxygen carrier supported for CLC using liquid fuel. The Thesis is composed with five chapters, Introduction being the

first Chapter. Chapter 2 summarizes the previous studies about chemical looping combustion and presents former research results regarding different oxygen carriers. Chapter 3 describes the experimental works while Chapter 4 shows the experimental methods used in this study. Finally, Chapter 5 presents the results and discusses how the data obtained from experiment is in satisfactory agreement with literature studies, followed by conclusion and recommendations.

CHAPTER 2

LITERATURE REVIEW

2.1 Oxygen Carriers

The oxygen carrier is the most important part of CLC unit. It the transfers oxygen from the air reactor and the fuel reactor. The key aspect of a successful CLC process is the performance of oxygen carrier.

In CLC, solid oxygen carrier is the source of oxygen for the combustion reaction. This reaction involves the interaction between the fuel and the active material. Therefore, the most efficient oxygen carrier should have a high concentration of active sites and well dispersed on the surface of the support. These properties are affected by the preparation method. Different methods have been used for preparing oxygen carrier, with incipient impregnation, spray drying and freeze granulation the most popular (Adanez et al., 2004).

In the process of preparing oxygen carriers, inert materials are usually used as supports for the active metal oxides. Supports are usually a porous material having a high specific area. Other characteristics of porous material include pore size and pore size distribution. (Cavani & Trifiró, 1997) summarized the major advantages of a support in the following:

a- Increase the mechanical resistance.

b- Increase the metal dispersion due to high surface area.

c- Stabilize the metal particle size.

Different materials have been used as a support includes: silica, alumina, zeolites.
Metal Dispersion is one of the fundamental characteristics of the supported metals. (Perrichon, Retailleau, Bazin, Daturi, & Lavalley, 2004).

CLC was not introduced initially to capture CO_2 but to enhance the efficiency of the power plants by (HORST J. RICHTER & KARL F. KNOCHE, 1983). They showed that if direct contact of fuel with oxygen is avoided, the irreversible entropy production of combustion can be decreased which will enhance the overall efficiency.

The first study for CLC as an alternative combustion method was done by Ishida and coworkers at Tokyo Institute of Technology (Ishida, Jin, & Okamoto, 1996). In this study, NiO was examined as oxygen carrier using methane as fuel. The result for this research was promising and showed great potential such that the power plants in the future will be able to use this new combustion method, and accordingly can lead to CO_2 capture. Another important study was done by Ishida in 1998 regarding carbon deposition on the oxygen carrier, in order to apply CLC in power plants. For different oxygen carrier, the kinetic behavior of carbon deposition was investigated using different fuels (Ishida, Jin, & Okamoto, 1998). The result of this study revealed the conditions in which coke formation can be controlled. Thus, the idea of utilizing power plants using CLC was thought to be feasible.

2.2 Development of Oxygen Carrier

In the most recent two decades, various establishments have started working in oxygen carrier improvement research. Most of the oxygen carriers are synthetic. However, natural oxygen carrier such as ilmenite ($FeTiO_3$) has also been studied (Liu et al.,

2013).The evaluation of oxygen carrier has been done in micro reactors or bench scale reactors using different fuels. The next two subsections will give a brief literature review for iron and manganese based oxygen carriers.

2.2.1 Fe-based oxygen carriers

Fe-based oxygen-carriers are an attractive choice for CLC process because of its low cost and environmental compatibility. Different oxidation states can be found For Fe-based oxygen-carriers when Fe_2O_3 is reduced (Fe_3O_4, FeO, or Fe). Only (Fe_2O_3-Fe_3O_4) transformation is applicable for industrial CLC due to thermodynamics limitation (Abad, Mattisson, Lyngfelt, & Rydén, 2006).

Fe_2O_3 with 60% loading supported on Al_2O_3 prepared by freeze granulation have been studied at temperature from 800 to 950 ^{0}C by (Abad et al). Evaluation of the prepared oxygen carriers were carried out in 300 W_{th} continuous unit using syngas or natural gas as a fuel. After 40 hours in combustion conditions, no sign of agglomeration, carbon deposition and deactivation where better results was for syngas than methane (Abad et al., 2006).

Lyngfelt and Thunman investigated iron oxide in a 10 kW_{th} CLC pilot plant. During 17 h of continuous operation and using methane as fuel, similar results were found in this pilot plant to that mentioned above done by Abad. 2-8 % CH_4 and CO outlet concentration were found even when working at low fuel rate. Son and Kim (Son and Kim, 2006) examined Fe_2O_3/bentonite oxygen carrier in kW_{th} CLC unit and similar conclusion were reached (Lyngfelt & Thunman, 2005).

Iron based was prepared by impregnation on alumina and tested in a 500 W_{th} CLC pilot plant at temperature of 880 ^{0}C (Ortiz et al., 2010). The results showed that no carbon

formation or agglomeration and complete combustion was obtained during 50 hours of combustion condition.

Iron oxides has been used in the application of CLC to solid fuels. Different solid fuels have been examined for CLC process where Fe2O3 is used as oxygen carrier. good performance was found with Fe2O3/MgAl2O3 in a batch fluidized bed (Leion, Mattisson, & Lyngfelt, 2007) whereas lower reactivity obtained when pure Fe2O3 powder is used without a support (Dennis, Scott, & Hayhurst, 2006).

2.2.2 Manganese-based Oxygen Carriers

Development of manganese oxide for the CLC process is considered attractive due to the low cost and nontoxic properties which is similar characteristics to the Fe-based materials. Moreover, manganese based oxygen carriers have higher oxygen transport capacity compered to iron based. However, just few works have been done regarding using manganese oxides as oxygen carriers. This study will examine the reactivity and stability of manganese based oxygen carrier.

Manganese oxide exhibits several oxidation states. MnO_2 is the highest oxidized manganese compound which decompose to Mn2O3 at a temperature around 500 ^{o}C (Stobbe, De Boer, & Geus, 1999)

Manganese based oxygen carriers have studied as pure manganese oxide and supported on inert materials. Low reactivity was found when pure manganese oxide is used (Siriwardane, Tian, Richards, Simonyi, & Poston, 2009)

Several support material have been used to enhance its performance. The use of bentonite as support in TGA reactivity test showed good results where syngas was used as a fuel (Tian, Simonyi, Poston, & Siriwardane, 2009). However, the use of $MgAl_2O_4$,

SiO_2 or TiO_2 as inert material revealed poor result due to the formation of unreactive phases which results from the high support metal interaction (Adanez et al., 2004; Stobbe et al., 1999).

Zirconia have been used as a support for manganese based oxygen carrier and showed high tendency for agglomeration (Marcus Johansson, Mattisson, & Lyngfelt, 2006) . To avoid this problem, the effect of some promoters to the zirconia support has been studied by Johansson et al. In this study, ZrO_2 stabilized by CaO, MgO or CeO_2 were prepared where the fuel is 50% CH4 and 50% H2O (M. Johansson, Mattisson, & Lyngfelt, 2006) . The addition of these promotors showed high reactivity and avoidance of agglomeration and Mg-ZrO_2 was the best among the different supports. Also, the effect of the sintering temperature was investigated. In this study, reactivity was inversely proportional to the sintering temperature.

Manganese oxide with alumina as a support have been prepared and evaluated for CLC by Mattison. It was evaluated at a temperature range 750-950 ^oC and using 29.4 wt % metal content. The extent of the reaction was limited due to the high support manganese oxide interaction (Mattisson, Järdnäs, & Lyngfelt, 2003). This reaction result in the formation of manganese aluminate according to this reaction:

$$MnO + Al_2O_3 \longrightarrow MnAl_2O_4$$

Manganese oxide, supported on Mg-ZrO_2 has been also investigated in the chemical looping combustion process using syngas as fuel. It was composed of 40% Mn_3O_4 and 60% Mg-ZrO_2, prepared by freeze granulation and sintered at 1423 K. 99.9% combustion efficiency was obtained in the temperature of 1073–1223 K with observing of absence of agglomeration and low attrition (Abad et al., 2006). Table 2.1 shows a

summary of the previous studies of Mn-based oxygen-carriers.

Table 2.1 Summary of Mn-based oxygen-carriers

Oxygen Carrier	**Fuel**	**Reference**
MnO_2	CH_4	(Roux, Bensakhria, and Antonini 2006)
Mn_2O_3	Coal	(Siriwardane et al. 2009)
46% $Mn_2O_3/MgAl_2O_4$	CH_4	(Zafar, Mattisson, and Gevert 2006)
40% Mn_2O_3/Bentonite	Syngas, Syngas +H_2S	(Tian et al. 2009)
47% Mn_2O_3/SiO_2	CH_4	(Zafar, Mattisson, and Gevert 2006)
37%Mn_3O_4/Al_2O_3	CH_4	(Adanez et al. 2004)
40%Mn_3O_4/Mg-ZrO_2	Natural gas, Syngas	(M. Johansson, Mattisson, and Lyngfelt 2006)
60%$Mn_3O_4/MnAl_2O_4$	CH_4	(Cho, Mattisson, and Lyngfelt 2004)
37%Mn_3O_4/Sepiolite	CH_4	(Adanez et al. 2004)
37%Mn_3O_4/ SiO_2	CH_4	(Cho, Mattisson, and Lyngfelt 2004)
37%Mn_3O_4/ TiO_2	CH_4	(Adanez et al. 2004)
37%Mn_3O_4/ZrO_2	CH_4	(Marcus Johansson, Mattisson, and Lyngfelt2006)
40%Mn_3O_4/ZrO_2-Ca	CH_4	(M. Johansson, Mattisson, and Lyngfelt 2006)
40%Mn_3O_4/ZrO_2-Ce	CH_4	(Marcus Johansson, Mattisson, and Lyngfelt 2006)

2.3 Chemical-Looping Combustion of liquid fuels

Most of the work to the date on CLC has been focused on solid and gaseous fuels such as coal, methane, natural gas, syngas etc. There are only limited studies used liquid fuels in CLC. Liquid fuels are gaining wide interest in the application of CLC in the oil and refining industry due it's attractive for transportation. According to EIA, Saudi Arabia is the top producer of liquid fuels in the world as seen in Fig 2.1.

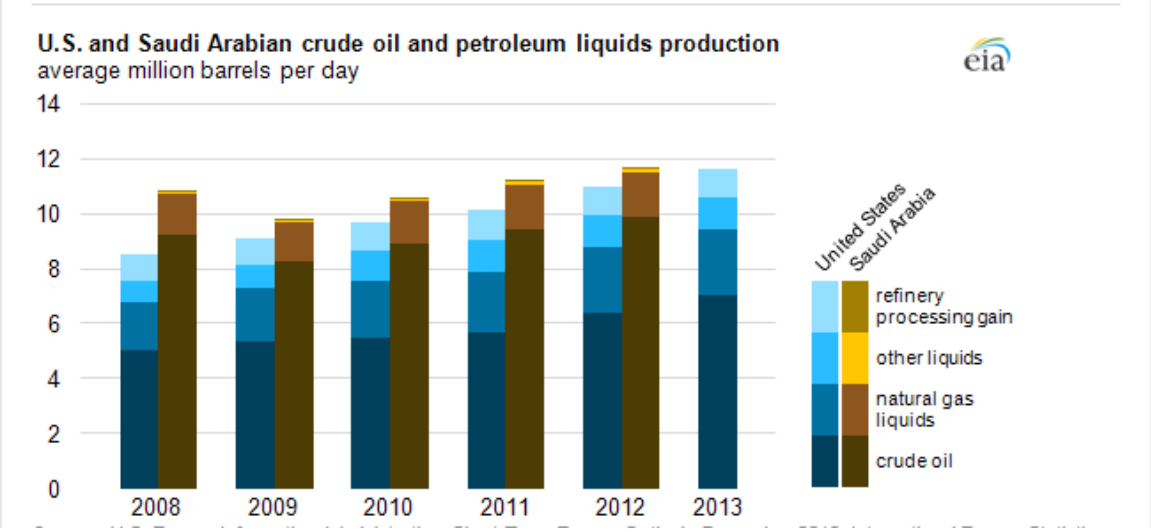

Figure 2.1 Production capacity of Saudi Arabia of liquid fuels (Source: U.S. Energy Information Administration)

However, the use of liquid fuels raises some difficulties in the application of CLC. The fuel here is evaporated first, and then mixed with the oxygen carrier. In the evaporation of liquid fuels, surface area-to-volume ratio is maximized which lead to the enhancement of the combustion rates. According to Magnus Ryden, the most important challenges when using heavy fuel oil as fuel in chemical-looping combustion is injection and vaporization of fuel directly into a fluidized bed since thermal decomposition and char formation could be expected to take place (Rydén et al., 2013). There are few studies for liquid fuels

applied to CLC (Moldenhauer et al., 2014)

Kerosene was studied as fuel for CLC (Rydén et al., 2013). In this study, kerosene was gasified before the combustion step. The products of the gasification process were mainly CO and H_2 before being oxidized in the fuel reactor. Bitumen and asphalt have been studied in CLC using copper-based oxygen carrier. The fuels were gasified before injecting to the reactor (Cao et al., 2011).

Chemical-looping combustion experiments were conducted using different grades of heavy oil using nickel oxide (Forret et al., 2009). Other groups have reported the work with liquid fuels in processes related to chemical-looping combustion including (Pimenidou, Rickett, Dupont, & Twigg, 2010) were waste cooking oil was used as fuel in a batch packed bed reactor. More research is required to investigate liquid fuels.

Moldenhauer et al examined a nickel-based oxygen carrier where kerosene is added to the fuel reactor directly (Moldenhauer et al., 2012). The fuel was gasified before feeding to the reactor. Nearly complete fuel conversion was achieved using nickel-based oxygen carrier composed of 40 wt% NiO and 60 wt% MgO–ZrO_2. In 2014, the same group investigated the performance of calcium manganite and ilmenite based oxygen carriers using fuel oil as a liquid fuel where the fuel is also injected to the fuel reactor. The results showed that most of the fuel carbon was converted to CO_2 and below 1 mol % carbon leakage was detected in the air reactor (Moldenhauer et al., 2014)

In this study, manganese oxide supported on alumina was used as oxygen carrier with liquid fuel. n-hexane will be used as fuel with different manganese loading. n-hexane is a liquid alkane hydrocarbon with the chemical formula C_6H_{14}.

CHAPTER 3

OBJECTIVES

The followings are the major objectives of this investigation

i. To develop Ce modified MnO_x/Ce-γAl_2O_3 oxygen carriers suitable for liquid fuel based chemical-looping combustion (CLC). The oxygen carriers are formulated to achieve optimum reactivity and oxygen carrying capacity in both liquid fuel and air during re-generation cycle.

ii. To study the liquid fuel (n-hexane) based CLC reactions under fluidized conditions in order to determine the best reaction conditions for complete fuel combustion.

iii. To investigate the solid-state kinetics of the reduction of the newly developed MnO_x/Ce-γAl_2O_3 oxygen carriers.

The following has been identified as the specific objectives to achieve the major objectives:

- Preparation of Ce modified MnO_x/Ce-γAl_2O_3 oxygen carriers using dry impregnation method with varied composition of manganese.
- Characterization of the prepared oxygen carriers using temperature programmed reduction, temperature programmed desorption, nitrogen adsorption and BET surface area analysis, X-Ray Diffraction, TGA, SEM-

EDX,

- Evaluation the reactivity of the prepared oxygen carriers in a fluidized CERC Riser Simulator using n-hexane as liquid fuel.
- Development of kinetics model for the reduction of oxygen carrier and estimation of the kinetics parameters.

CHAPTER 4

EXPERIMENTAL METHODS

4.1 Introduction

This chapter presents the experimental methods used in this study. This include three main sections: (i) oxygen carrier preparation, (ii) characterization and (iii) evaluation in a fluidized Riser Reactor Simulator. In section 4.2, a detailed description of the preparation steps is presented. Section 4.3 discusses various characterization techniques that were used. This include, XRD, TPR, TPD, TGA, SEM-EDX, and BET. In section 4.4, a description of the Riser Reactor which used to evaluate the oxygen carrier is provided.

4.2 Preparation of Oxygen Carrier

The wetness impregnation method is used to synthesize the MnO_x/Ce-γAI_2O_3. A commercial porous γ-Al_2O_3 as a support, while manganese nitrate (Mn $(NO_3)_2$. $5H_2O$) and cerium nitrate (Ce $N_3O_9.6H_2O$) were used as sources for manganese and cerium. The support was calcined at 500 °C in order to desorb the water.

The γ-Al_2O_3 is a metastable phase of α-Al_2O_3. At high temperature, the metastable phases are implicated to a phase change ending to the stable α-Al_2O_3 phase (Wallin, Andersson, Chirita, & Helmersson, 2004). Comparing the surface area, γ-Al_2O_3 have much bigger surface area than α-Al_2O_3 which make the formation of α-Al_2O_3 unfavorable. In order to enhance the γ-Al_2O_3 thermal stability, alkali and rare earth metal oxides usually added to the support (Cui et al., 2015).

In this study, Ce modification is used to improve the thermal stability of the high surface area γ-Al_2O_3 by prevent it from converting to the low surface area alpha-phase as the temperature is raised (Singleton & Oukaci, 2001). A 1% of ceria was the optimum loading and overloading of cerium decreases the surface area of the alumina because of the growth of CeO_2 particles (Ozawa & Kimura, 1990). Also, the effect of cerium modification on the metal support interaction was studied.

The main steps involved in this method are: support impregnation, drying and reduction. In each Impregnation step, 5 wt. % Mn was added to the modified support. The loading were 5 wt. %, 10 wt. %, 15 wt. % and 20 wt. %.

The impregnation step was carried out in a quartz conical flask which is connected to a vacuum pump. The desired amount of Mn $(N0_3)_2.6H_20$ solution was prepared based on the pore volume of γ-Al_2O_3, 0.7 mL ethanol was used per gram of support. The nitrate solution was added drop by drop under continuous mixing and vacuum.

The resulting paste was dried at 110 C^0 over 3 hours and kept constant for 5 hours. After that, the sample was placed in a fluidized bed reactor up to 750 C^0 and kept constant for 8 hours with flow of 10% hydrogen and balanced argon gas mixture for the reduction step. Finally, the desired metal loading was calcined in air in the oven at 750 C^0 over 4 hours and kept constant for additional 8 hours.

4.3 Characterization of Oxygen Carrier

A variety of techniques were used for the characterization of the prepared oxygen carriers in this study. These characterization techniques used to understand the physical and chemical properties.

4.3.1 X-Ray Diffraction

XRD is used to identify the crystalline phases of the prepared samples. The limitation of XRD that amorphous and small particle phases will show no diffraction lines (Stock & Cullity, 2001). XRD was operated at 40 kV and 30 mA, employing Cu K α radiation (λ= 1.54 A^o). Bragg's law will be used to find the spacing distance d. Bragg's law is defined by the following equation:

$$n\lambda = 2d \sin(\theta)$$

where,

λ = the wavelength of the x-ray

d = the spacing of the crystal layers (path difference)

θ = the incident angle, n = an integer.

4.3.2 N_2 Adsorption

The adsorption of gases on a solid surface can be used to determine the total surface area of a material and pore volume. The experimental method widely used for the determination of surface area for porous materials is known as the BET (Kokes, Tobin Jr, & Emmett, 1955). The resulting BET equation is:

$$\frac{1}{v[(p_0/p) - 1]} = \frac{c - 1}{v_m\, c}\left(\frac{p}{p_0}\right) + \frac{1}{v_m\, c}$$

Where,

P = partial vapor pressure of adsorbate gas in equilibrium with the surface at 77.4 K (b.p. of liquid nitrogen).

P_o = saturated pressure of adsorbate gas.

V_a = volume of gas adsorbed.

V_m = volume of gas adsorbed at STP to produce an apparent monolayer on the sample surface.

C = dimensionless constant.

So, from the slope and y-intercept, V_m and C will be calculated and the specific area (m^2/g) is calculated. The specific surface area of the samples was determined in Autosorb (Quantachrome) analyzer by using N_2 adsorption at 77K. For each experiment, 0.1-0.2 g of sample was degassed at 573K for 2.5 h before analysis.

4.3.3 SEM-EDX

Scanning electron microscope (SEM) equipped with an energy dispersive X-ray spectrometer (EDX) was used to measure the surface compositions in the oxygen carrier and to evaluate the distribution of the components across the oxygen carrier surface. The scans were taken at 20 k eV voltage in low-vacuum mode with coating the nonconductive sample with sputtered gold. SEM images were also taken using the same microscope at 20 k eV beam voltage.

4.3.4 Temperature-programmed reduction (TPR)

TPR is widely used to determine the reducibility of the sample under a flow of hydrogen balanced in argon with linear increase in the temperature. Also, the reduction temperature is another important result from TPR.

TPR was operated at 50 cm^3/min STP with a heating rate of 10 C°/min and carried out in the range 30-850 C°. A typical TPR profile for the reduction of a metal oxide powder is displayed in Figure 4.1. The increase of voltage of the TCD is due to the change of

composition of the hydrogen of the exit stream gas passing through the TCD filament. The amount of hydrogen consumed is calculated by the area under the curve. The amount of hydrogen reacted can be related to the amount of reducible metal in the oxygen carrier sample using the following relation:

$$W_{Mn} = \frac{MW_{Mn} \times V_{H_2}}{v \times V_g}$$

Assuming that Mn_2O_3 is the initial reducible catalyst species present on the support, then the following reaction can be considered during the reduction of the sample:

$$Mn_2O_3 + H_2 \rightarrow 2\ MnO + H_2O$$

The reduction percentage can be now calculated by the following equation:

$$f = \frac{W_{Mn}}{W_0}$$

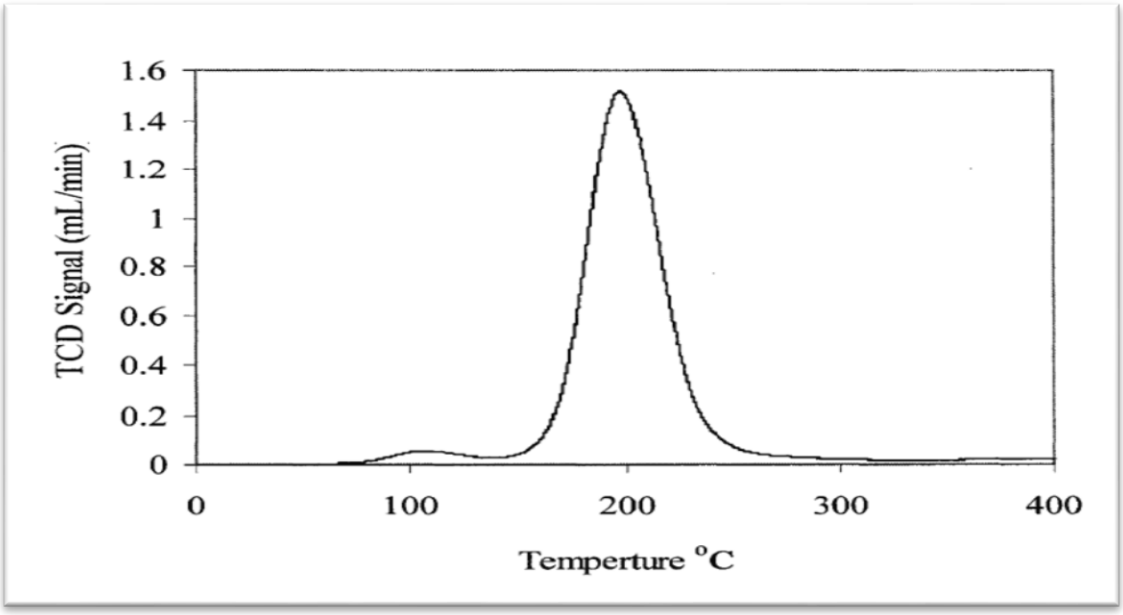

Figure 4.1 Typical TPR profile for the reduction of a metal oxide powder (reference)

4.3.5 Temperature programmed desorption (TPD)

TPD technique is important for the determination of kinetic and thermodynamic parameters of desorption processes. A sample is heated with a temperature program $\beta(t) = dT/dt$ which means that the temperature T being a linear function of the time t (Neurock, 1994). TPD was operated at 50 cm^3/min STP with a heating rate of 10 C°/ min and carried out in the range 30-600 C°.

Micromeritics AutoChem II 2929 analyzer was used for TPR and TPD experiments. Figure 4.2 shows the schematic diagram of AutoChem II. The experiments are based on the following simplified steps (AutoChem II 2920 analyzer manual):

(i) Gas flows into the analyzer

(ii) Gas interacts with the sample as the temperature changes

(iii) Gas flows past the detector

(iv) Detector (TCD) collects data

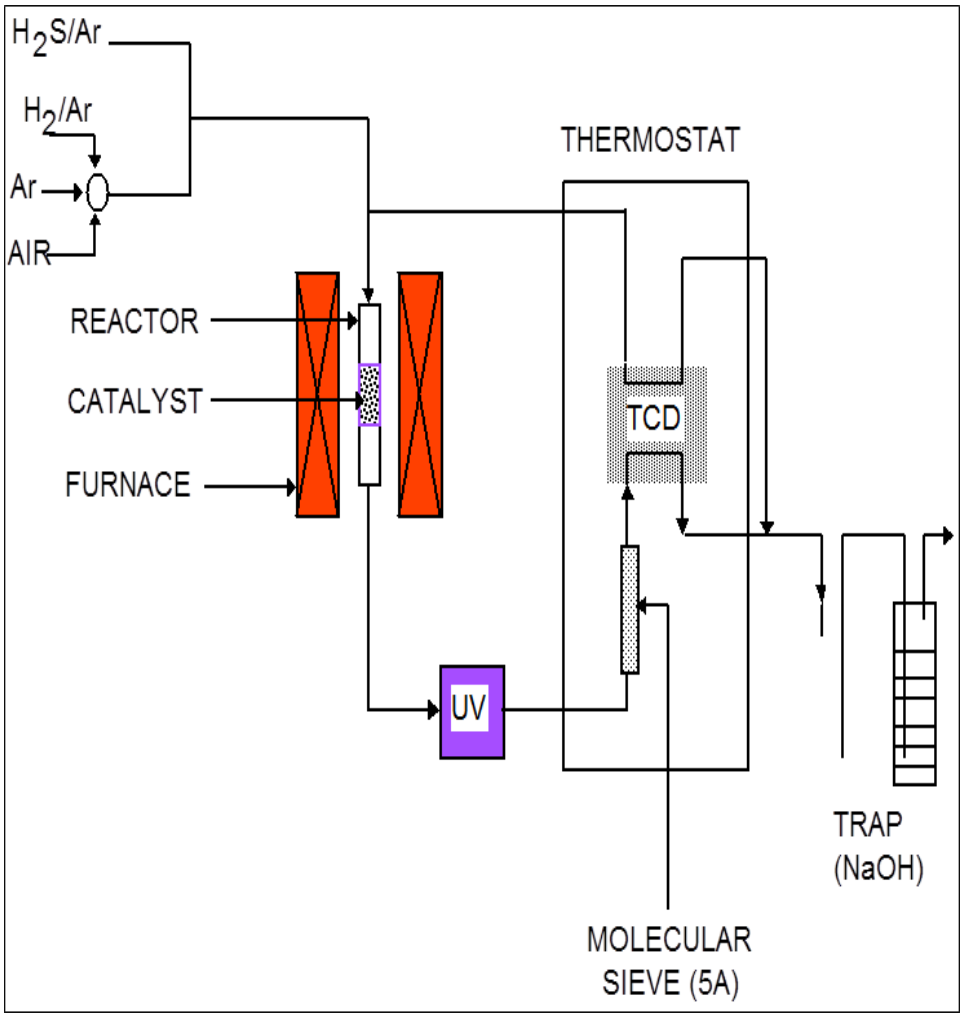

Figure 4.2 Micrometrics AutoChem II schematic diagram

4.3.6 Thermogravimetry analysis (TGA)

TGA is one of the most used techniques in thermal analysis, in which changes in the sample mass under a programmed temperature change is recorded as a function of temperature or time (Kemp, 1999). Measurements are usually conducted in inert gas (He, N2, Ar) atmosphere, although reactive gases, such as hydrogen or oxygen can be used when studying sample weight loss under reducing or oxidizing conditions.

Thermogravimetric analysis was carried out on TGA - SDT Q600 under nitrogen inert atmosphere flowing at 50 ml/min. Figure 4.3 shows the schematic diagrams of the TGA - SDT Q600.

Figure 4.3 Photograph of the TGA - SDT Q600

4.4 Evaluation of oxygen carrier

The oxygen carriers prepared in this study were evaluated by using the CREC Riser Simulator. Figure 4.4 shows the schematic diagrams of the CREC Riser Simulator and its components. The CREC Riser Simulator is a fluidized reactor of the batch type with internal recycle. It has two sections: a lower section and upper section. There is also an annular spacing between the basket and the internal cavity of the reactor. Rotation of the shaft and impeller promotes a low pressure point in the upper section of the basket. This promotes an upwards gas motion in the central section and a down flow gas circulation in the outer section. As a result, the oxygen carrier is fluidized.

The CREC Riser Simulator operates in conjunction with some other accessories, such as a vacuum box, a gas chromatograph (GC), and series of sampling valves, a timer, two

pressure transducers and two temperature controllers. A schematic diagram of the CREC Riser Simulator experimental set-up used in this study is shown in Figure 4.5.

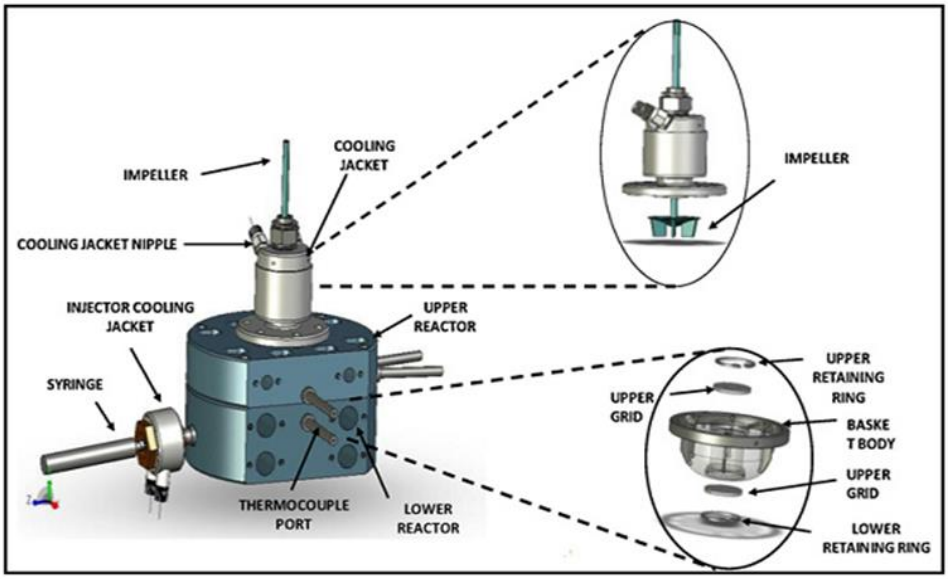

Figure 4.4 Schematic diagrams of the CREC Riser Simulator (Hossain et al 2007)

For each reaction run, the required amount of oxygen carrier sample was first loaded into the reactor basket and then the reactor was closed. The temperature program was run to heat up the system to the desired reaction temperature. An argon flow was maintained in the system to ensure that the system was free from any gaseous oxygen (air). Once the reactor reached thermal equilibrium at the desired temperature, the argon flow was stopped and the vacuum box pressure was reduced to 20.7 kPa using a vacuum pump. At this stage, the impeller was turned on and the feed (C_6H_{14}) was injected into the reactor using a preloaded syringe.

During the reaction period, the pressure profile of the reactor was recorded using a pressure transducer. The reactor pressure increased as soon as the reaction proceeded, given the increased number of moles in the gas phase due to the reaction. At the end of

the pre-specified reaction time, the isolation valve between the reactor and the vacuum box was opened and the pressure was reduced to the value of the vacuum box pressure. Finally, the product gas is analyzed by gas chromatography (GC) with thermal conductivity detector (TCD) and a flame ionization detector (FID).

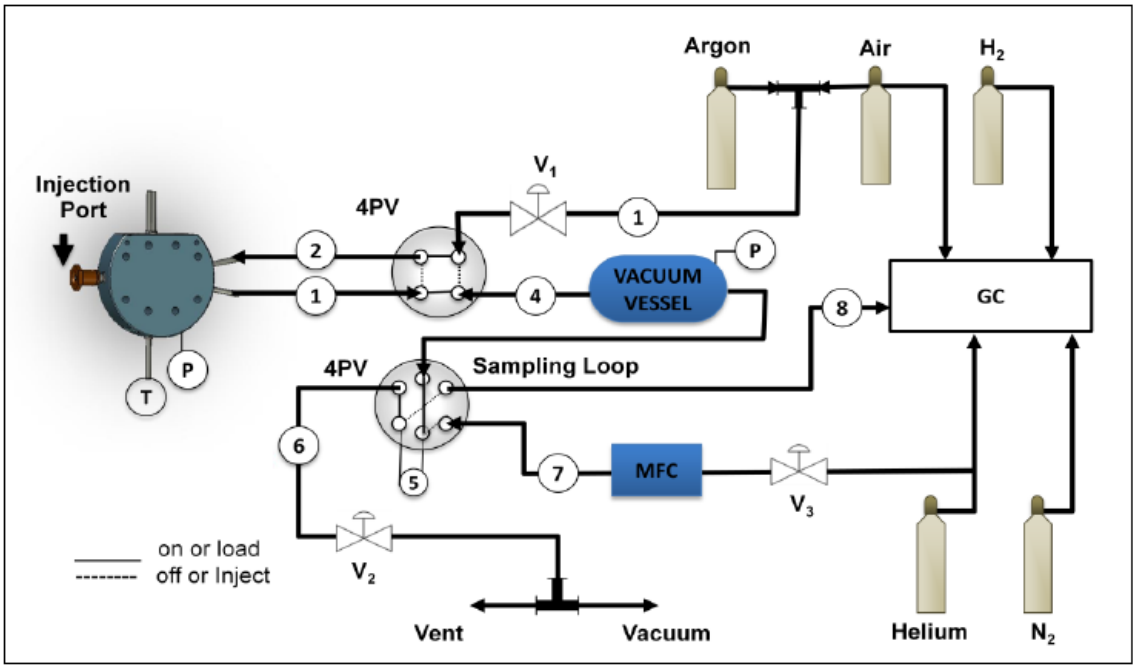

Figure 4.5 CREC Riser Simulator Schematic diagram of the experimental set-up (Hossain et al 2007)

CHAPTER 5

RESULTS AND DISCUSSION

5.1. Introduction

This chapter presents the experimental results of ceria promoted oxygen carrier studied in this study. There are three major sections of this chapter: (i) characterization of the prepared Ce modified Mn based oxygen carriers and (ii) evaluation of the oxygen carriers and (iii) kinetics modeling of the reduction kinetics of the oxygen carrier.

5.2. Characterization

5.2.1. Metal Loading and dispersion

The oxygen carrier samples were prepared using incipient impregnation with different manganese loading Ce modified over gamma alumina support. The manganese loading was varied from 5 to 20 wt.% of while Ce loading was kept at 1 wt %. Before the Mn loading, the support $\gamma Al2O_3$ was modified with 1 wt. % Ce. The prepared oxygen carrier samples were analyzed using both XRF and SEM-EDX in order to confirm the desired metal loading. Table 5.1 shows the targeted and actual metal loading as measure by XRF analysis. On can see from Table 5.1, the measured actual metal compositions measured by XRF are in excellent agreement with the targeted compositions. Expectedly, the metal loading measured by EDX shows some variations given it measures the composition based on surface metals.

Figure 5.1 shows the dispersion of the manganese species over the Ce-modified alumina support. The obtained imaging is dependent on atomic number contrasts among the different constituents of the sample, which indicates the bright zones represent heavy elements while the dark zones correspond to light elements. Thus, the bright zones can be assumed as manganese oxide species and the dark ones as the support.

Table 5.1 Metal loading analysis of the prepared oxygen carrier

Sample	Ce loading (wt %)			Mn loading (wt %)		
	Targeted	EDX	XRF	Targeted	EDX	XRF
5% MnO_x/Ce-γAl_2O_3	1	0.74	0.99	5	4.9	4
10% MnO_x/Ce-γAl_2O_3	1	0.63	0.96	10	6.5	8
15% MnO_x/Ce-γAl_2O_3	1	0.63	1.18	15	9.8	13
20% MnO_x/Ce-γAl_2O_3	1	0.48	1.2	20	18.8	15

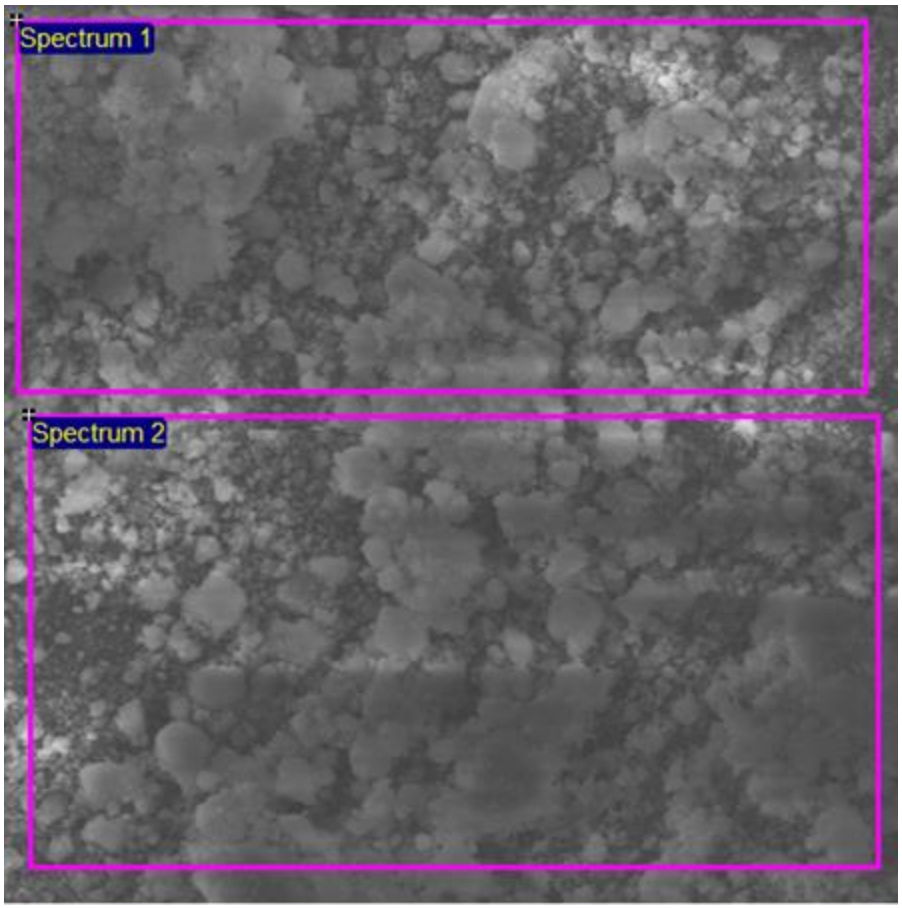

Figure 5.1 Scanning electron micrographs of a fresh oxygen carrier sample

5.2.2. X-ray diffraction

X-ray diffraction was used to determine the bulk crystalline phases in the samples. Also, XRD is used to observe the alumina phase and manganese oxide phase present in the prepared oxygen carriers. XRD was operated at 40 kV and 30 mA, employing Cu K α radiation (λ= 1.54 A^o). Scherrer's equation was used to find the crystallite size. Scherrer's formula is defined by the following equation:

$$D_p = \frac{0.94\lambda}{\beta_{1/2}\cos\theta}$$

where, D_p = Average Crystallite size,

β = Line broadening in radians.

θ = Bragg angle.

λ = X-ray wavelength

Figures 5.2 shows the XRD patterns of the bare γ-Al_2O_3 support and prepared Ce modified MnOx/Ce-γAl_2O_3 oxygen carrier samples. The main diffraction angles of γ-Al_2O_3 at 37.11°, 45.5°,and 66.8° which correspond to (311), (400) and (440) diffraction planes. This diffraction was compared with the standard powder diffraction of the International Centre for Diffraction Data (ICDD) database for gamma alumina (Figure 5.3). The comparison reveal that no phase change and the high surface area γ-Al_2O_3 cubic structure is maintained. This is in agreement with studies performed by (Peluso, Pronsato, Sambeth, Thomas, & Busca, 2008) .

5 % MnO_x/Ce-γAl_2O_3 and 10 %MnO_x/Ce-γAl_2O_3 show no diffraction peak for any manganese species. The only peaks appeared for these samples are γ-Al_2O_3 peaks. This is explained by either amorphous manganese oxide formation- which is highly dispersed- or by the formation of XRD undetectable manganese oxide crystallites. XRD detect crystalline particles with more than 5 nm crystallite size (Álvarez-Galván, de la Peña O'Shea, Fierro, & Arias, 2003a). However, the X-ray spectrum of 15MnOx/ γ-Al_2O_3 and 20 MnOx/ Ce-γAl_2O_3 shows a signal for Mn_2O_3 peak at 2θ = 37 based on the ICDD reference. This peak is overlapped with γ-Al_2O_3 at the same diffraction angle. Furthermore,

the intensity of Mn_2O_3 for 20 Mn loading is sharper than 15 Mn with smaller broadening indicating the larger crystallite size. Using Scherer's equation, the crystallite size of Mn_2O_3 for 20Mn and 15 Mn are 5.35 nm and 4.51 nm respectively.

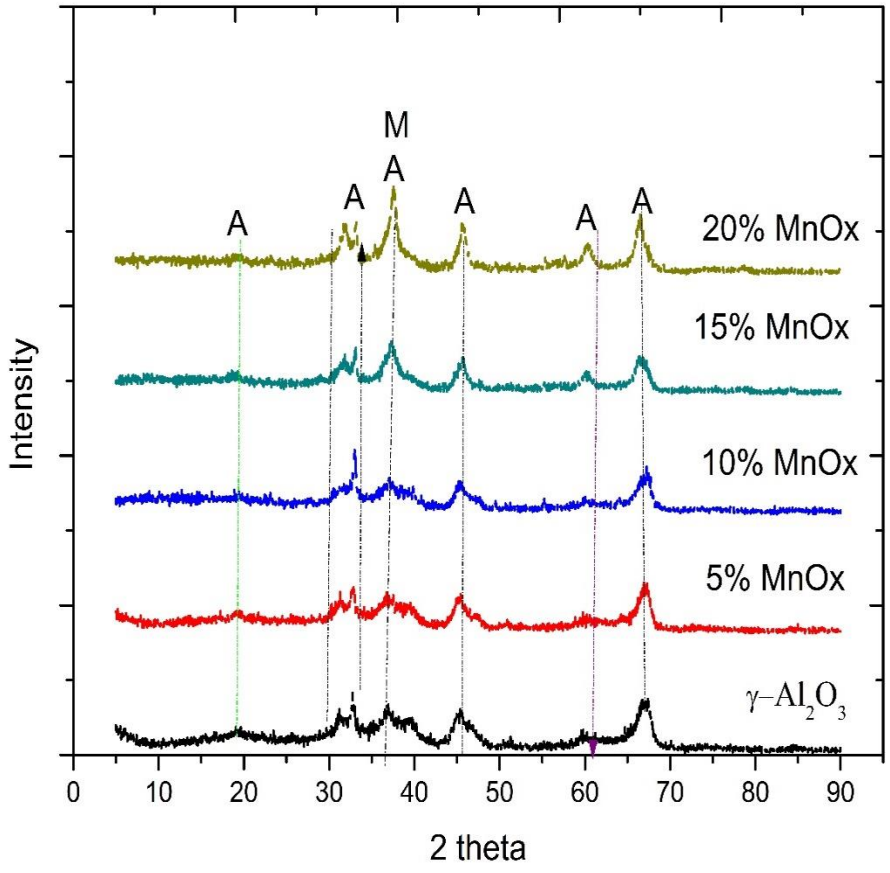

Figure 5.2 X-ray diffraction of γ-Al_2O_3 and supported manganese oxide. A: γ-Al_2O_3, M: Mn_2O_3

Qualitative analysis results

Phase name	Formula	Figure of merit	Phase reg. detail	DB card number
gamma-Al2 O3	Al2 O3	1.558	ICDD (PDF2009)	00-050-0741
Bixbyite-C,	Mn2 O3	1.561	ICDD (PDF2009)	03-065-7467

Measurement profile

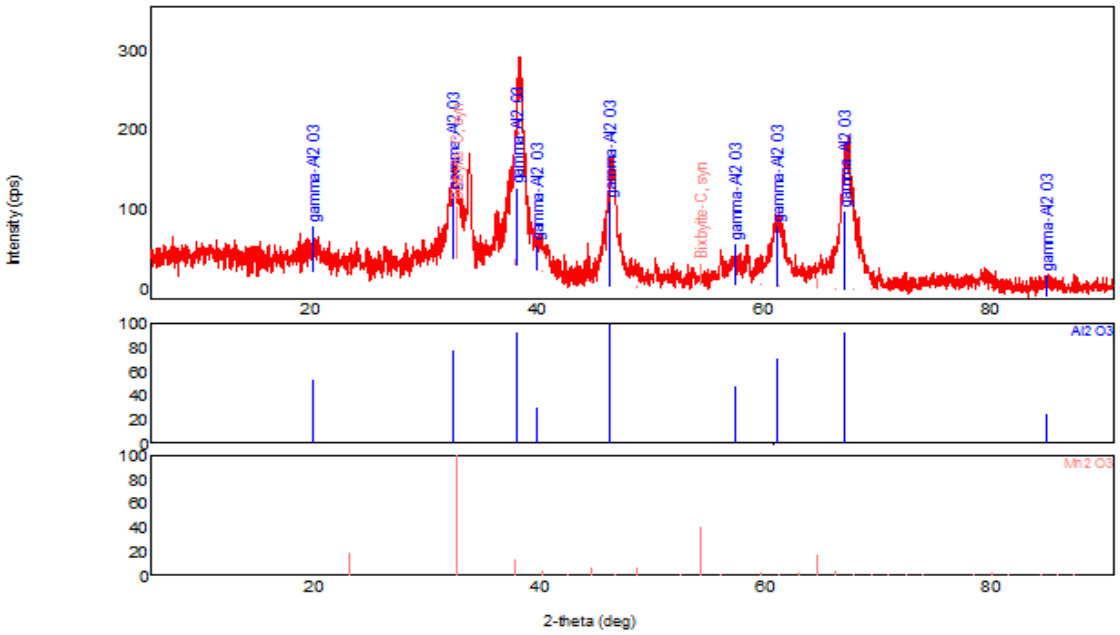

Figure 5.3 X-ray diffraction of MnO_x /γ-Al_2O_3 compared with ICDD reference

Also, the XRD patterns of supported manganese oxide over γ-Al_2O_3 shows no assigned peaks for the spinel structure $MnAl_2O_4$ which is difficult to be reduced.

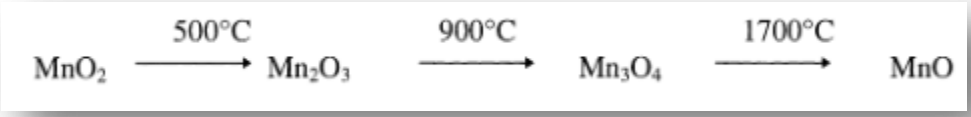

Figure 5.4 The manganese oxide phases at different temperatures.

Similar observation was reported elsewhere (Tao et al., 2014). Also, this result is consistent with studies performed by Stobbe and Boer which relate the manganese oxide

phase with the calcination temperature as seen in Fig 5.3. No CeO_2 peak is detected in XRD pattern. This result is expected due to low content of Ce in the sample.

Furthermore, no manganese aluminate formation detected by XRD for all the manganese loading. Manganese aluminate ($MnAl_2O_4$) have a spinel structure which is difficult to be reduced. Also, manganese aluminate appearance will result a decrease in the number of active sites (Cui et al., 2015). (Mattisson et al., 2003) prepared and evaluated supported Manganese oxide over alumina as a support for CLC. It was evaluated at a temperature range 750-950 ^oC and using 29.4 wt % metal content. The extent of the reaction was limited due to the interaction between the metal oxide and the alumina support. The XRD spectrum of the cerium modified manganese oxide supported on γ-Al_2O_3 oxygen carrier raveled the stable high surface area γ-Al_2O_3 after calcination at 750 ^0C. Also, no formation of the manganese aluminate indicating the negligible reaction between MnO_x and γ-Al_2O_3 at 750 ^0C in the presence of cerium promoter.

5.2.3. N_2 Adsorption

The surface area is a fundamental characteristic property involved in heterogeneous reactions. Also, the specific area is one of the important parameters to determine the degree of dispersion of the active material over the support. The specific surface area and pore volume were determined by the Brunauer-Emmet-Teller (BET) method using nitrogen physisorption at 77 k. The samples were vacuum degassed at 120°C for 3 hours prior to analysis. The adsorption/desorption isotherm for γ-alumina is shown in Figure 5.5. According to IUPAC, the reported isotherm is recognized as type IV isotherm which indicates a mesoporous pore size in the range of 2-50 nm. Moreover, the capillary

condensation starts from a relative pressure of 0.8. Also, 0.05 relative pressure difference was observed between the capillary condensation and capillary evaporation creating a hysteresis loop which indicate the mesoporous pore size.

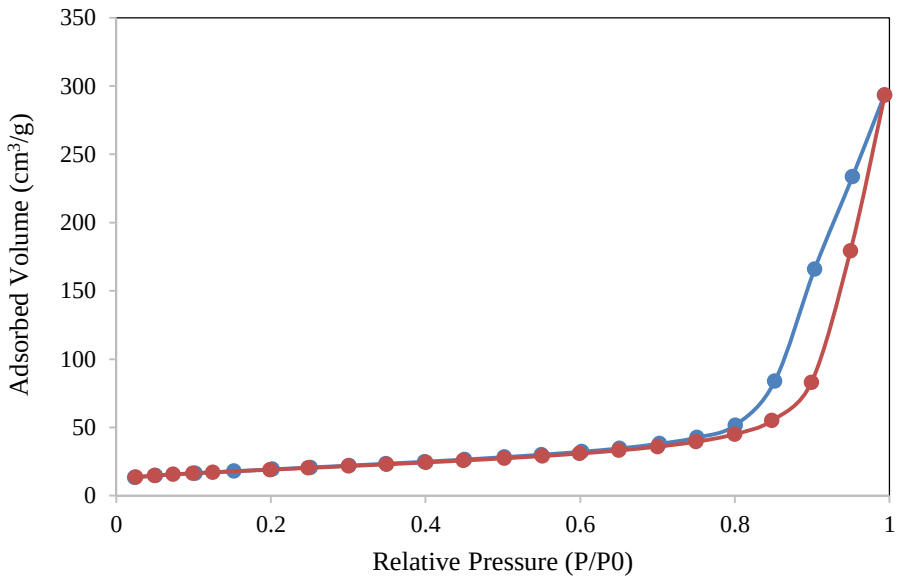

Figure 5.5 Adsorption/desorption isotherm of γ-Al_2O_3

Table 5.2 shows the surface area and pore volume of the γ-alumina support and supported manganese oxide samples. The specific surface area was found to be 132.03 m^2/g for the pure support γ-alumina. After 5% Mn loading, the specific surface area displaces a mild decrease to 102.10 m^2/g.

Furthermore, a gradual decrease was observed with increasing the metal loading. This result indicates that the surface area will be decreased as the metal loading increased. This reduction in the specific surface area is due to the change in the pore structure. The

same decreasing trend as the metal loading increased was found for the pore volume which is explained by the same reason.

Table 5.2 Surface area and pore volume of the prepared oxygen carrier

Oxygen Carrier	BET Surface area (m^2/g)	Pore volume (cm^3/g)
γ-Al_2O_3	132	1.0
5% MnO_x/Ce-γAl_2O_3	102	0.73
20% MnO_x/Ce-γAl_2O_3	91.4	0.62

5.2.4. Temperature Programmed Reduction (TPR)

TPR evaluation provides valuable information about the reduction characteristics of the oxygen carrier. Figure 5.6 shows the TPR profiles of supported manganese oxide. 20Mn/Al_2O_3 TPR profile a small broad peak at 330 C and strong symmetric peak at T=430 C. Based on XRD results, The first reduction step is attributed to Mn_2O_3 reduction to Mn3O4 while the second peak due to Mn_3O_4 reduction to MnO at a higher temperature.

However, the TPR profile for 15 Mn/Al_2O_3 shows only one broad peak at about 420 C. This indicates that the two reduction steps are lumped in a single peak which suggests the highly dispersed active sites over the support. Also, the reduction Temperature of 15 Mn/Al_2O_3 shifted slightly towards lower temperature compared with 20Mn/Al_2O_3. These findings suggests that sub-monolayer coverage with easily reducible species is formed for

15 Mn loading compared to 20 Mn loading. This is could be explained from the smaller crystallite size of 15 Mn compared to 20 Mn loading. Also, based on the surface area of the support and the theoretical size of manganese, the monolayer coverage is equivalent to 14.97 % Mn loading.

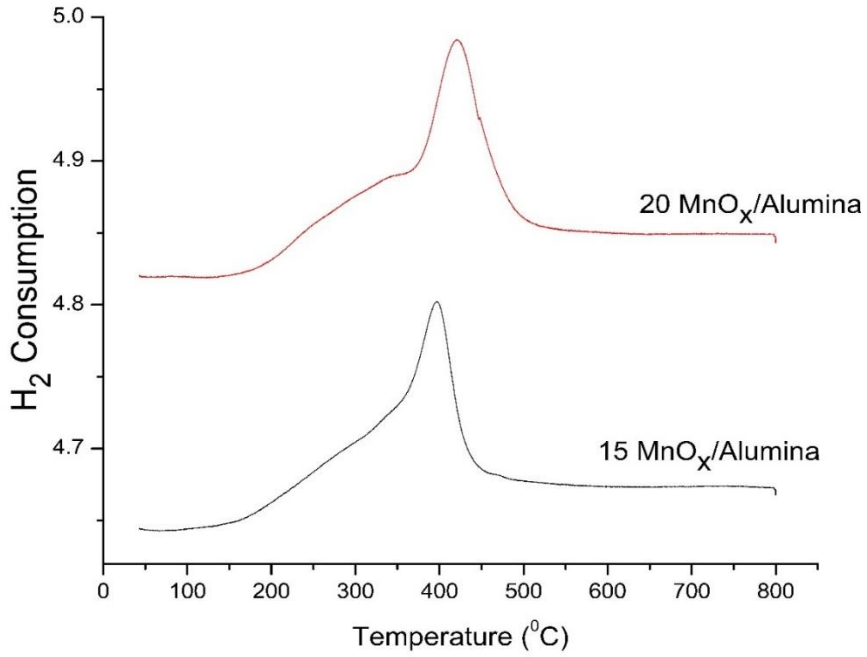

Figure 5.6 TPR profiles of different $MnO_x/Ce\text{-}\gamma Al_2O_3$ oxygen carriers

The TPR profile of pure manganese oxide supported on alumina was studied by (Álvarez-Galván, de la Peña O'Shea, Fierro, & Arias, 2003b). The result in this study shows two concentrated peaks at 330 and 405 ^{0}C Figure 5.7. These finding is similar to the bulk manganese oxide with small shift to lower reduction temperature. Similar observation was achieved by (Álvarez-Galván, Pawelec, de la Peña O'Shea, Fierro, & Arias, 2004). In a relevant study, (Hu, Chu, & Shi, 2008) studied a series of supported manganese oxide on alumina with different MnO_x loading ranging from 2 to 15 wt.% as

seen in Figure 5.8. The TPR profile was influenced by manganese loading and the peak area is increased as the loading increased.

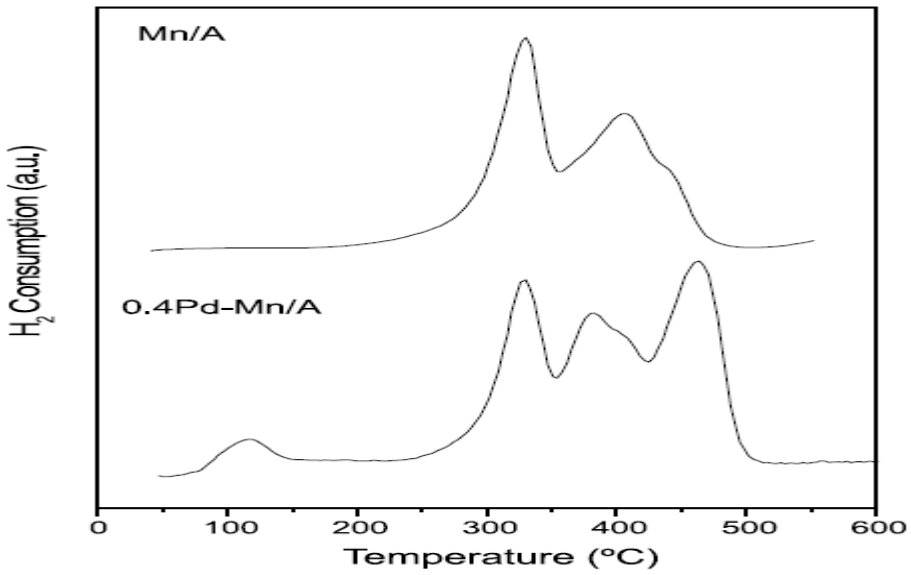

Figure 5.7 Temperature-programmed reduction profile of $Mn/\gamma Al_2O_3$ (Álvarez-Galván et al. 2003b)

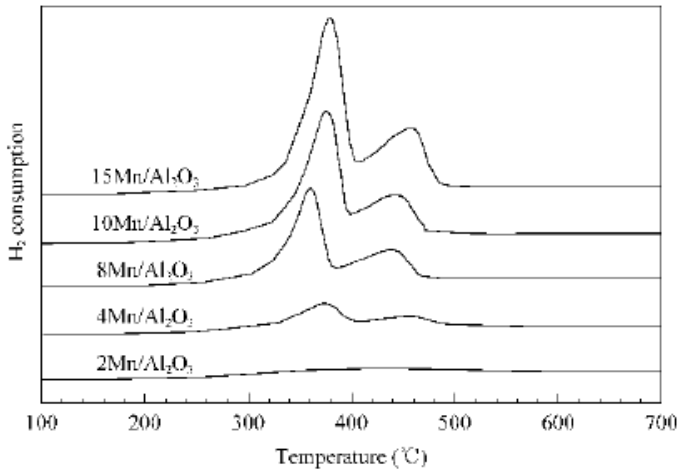

Figure 5.8 TPR profiles of the Mn/Al_2O_3 with different Mn loadings (Hu, Chu, and Shi 2008)

TPR data was used to use to calculate the reduction percentage from the hydrogen volume. The metal percentage reduction over repeated cycles is presented in Figure 5.9. More than 83 % metal reduction was stable over repeated cycles Figure 5.10.

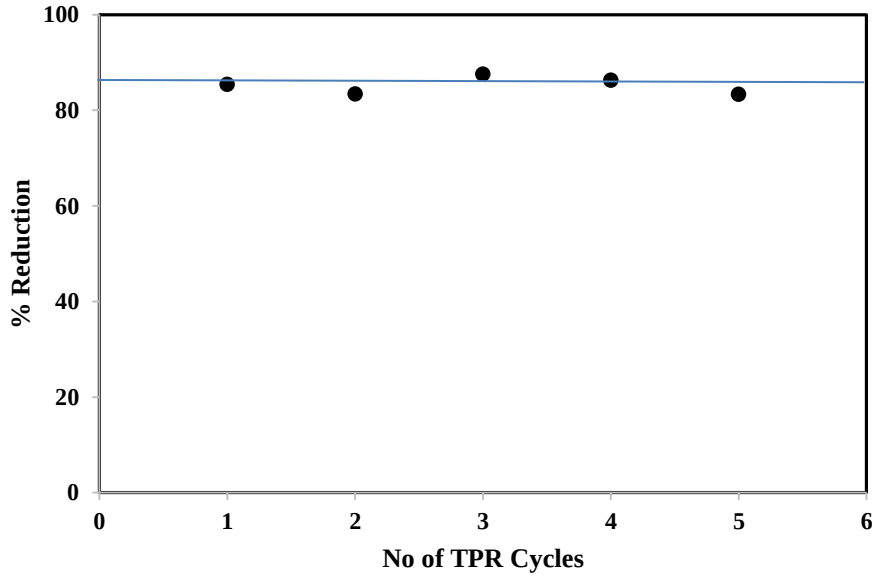

Figure 5.9 Reduction percentage of manganese based oxygen carriers over repeated TPR/TPO cycles

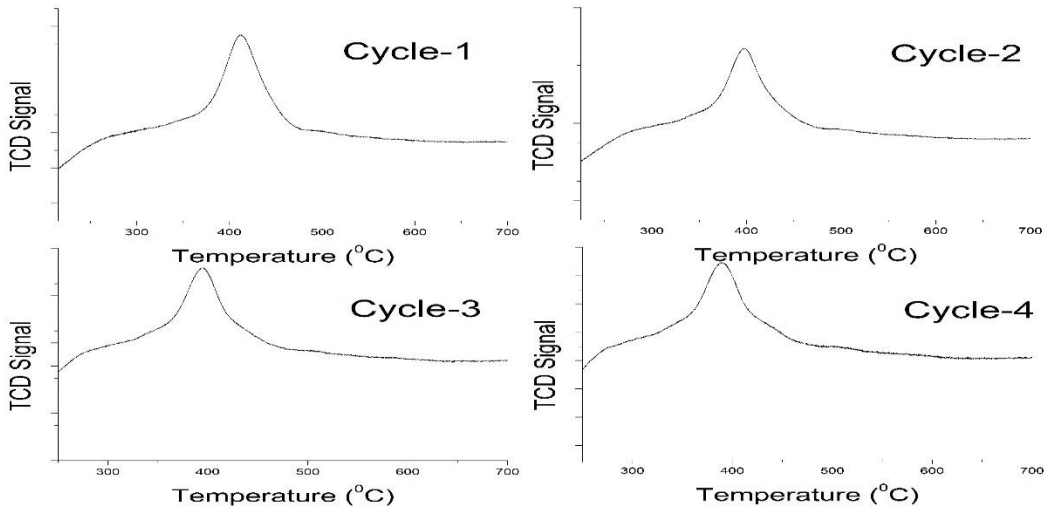

Figure 5.10 TPR profiles of manganese based oxygen carriers over repeated TPR/TPO cycles

5.2.5. Temperature Programmed Desorption (TPD)

NH3-TPD is used to study the acidity strength of the supported manganese oxide. Surface acidity is governed by the surface structure of surface manganese and the nature of the support used. The total acidity of γ-Al2O3 support and the MnOx/γ-Al_2O_3 samples with different manganese loadings were determined using NH_3-TPD. NH_3 is used as a basic probe molecule in TPD in order to determine the strength of acid sites. Ammonia is used due to its small dimension which make all the OH groups accessible through the pores (Chester & Derouane, 2009). From the peak area and the desorption temperature, the acid amount and acid distribution are obtained.

Figure 5.11 shows the TPD profile of γ-Al_2O_3 and cerium modified γ-Al_2O_3 where NH3 pre-adsorbed at 120 ^{0}C with a linear increase in temperature (10 ^{0}C/min). One can see

from the TPD profile that cerium modification affects metal-support interaction. Ce introduction to alumina created a bigger weak acid sites at 240 ^{0}C while the same peak at 560 ^{0}C.

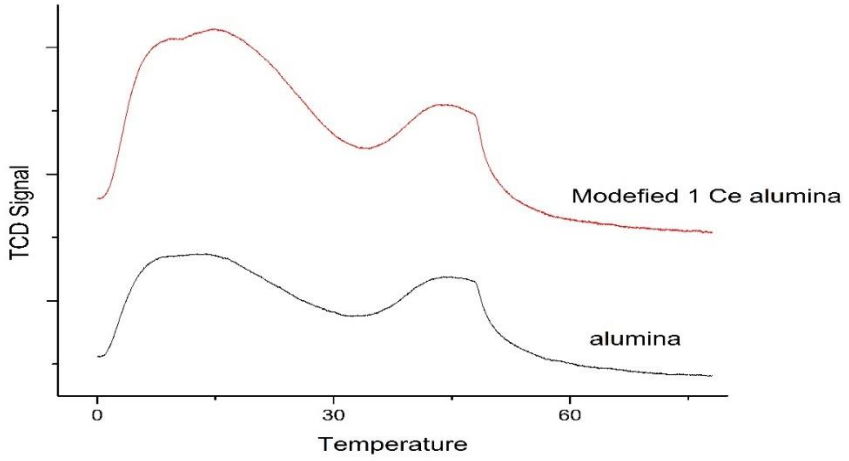

Figure 5.11 TPD profiles of γ-Al_2O_3 and cerium modified γ-Al_2O_3

Also, Fig. 5.12 shows the TPD profile of 15 γ-Al2O3 and 20 Mn /γ-Al2O3. Two peaks at 180 and 592 ^{0}C. It appears that manganese loading reduces the sample acidity as in Table 5-3. This attributed to the acid sites blocking *(Anna Galiková, n.d.)*. However, the acidity of 15Mn is slightly lower than 20 Mn which is a result of low dispersion of 20 Mn compared with 15 Mn. Moreover, the temperature for the strong acidity peak is shifted to a higher temperature in Mn 15 compared to Mn 20. This indicates that metal support interaction is higher in Mn 15. Metal support interaction has to optimized to be a moderate interaction to ensure the high dispersion and prevent the formation of difficult reducing manganese aluminate *(Cui et al., 2015)*.

Table 5.3 NH_3-TPD uptake of MnO_x/Ce-γAl_2O_3 samples

Sample	NH_3 Uptake (cm^3 STP/g)
1% Ce-Al_2O_3	16.1
15% MnO_x/Ce-γAl_2O_3	8.5
20% MnO_x/Ce-γAl_2O_3	9.8

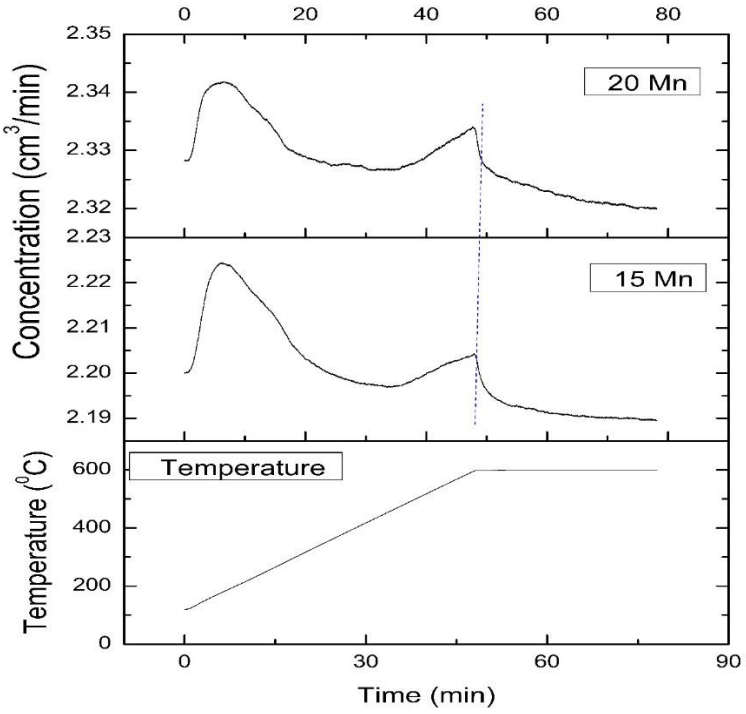

Figure 5.12 TPD profile of γ-Al_2O_3 supported manganese oxide

5.2.6. Thermogravimetry Analysis

Thermogravimetric analysis was carried out on a SDT Q600 under nitrogen inert atmosphere flowing at 50 mL/min. In each run, 15 mg of the sample was heated from room temperature to 1000 °C at a heating ramp rate of 20°C/min with recording the weight change in the oxygen carrier sample. Figure 5.13 presents the TGA profile for 20 MnO_x/gamma alumina oxygen carrier. It can be noticed that the most loss in the weight

occurs below the 200 C due to the desorption of water. This is confirmed from the derivative weight profile where the maximum weight change occurs at 100 °C.

The result from the TGA indicates the reaction mechanism between the vaporized fuel and the oxygen carrier to be a solid gas reaction in the fuel reactor. The process where the metal oxide releases oxygen in the gas phase is called chemical looping with oxygen uncoupling. Different materials have been identified to be suitable for CLOU process include CuO/ Cu_2O and Co_3O_4/CoO (Mattisson, Lyngfelt, & Leion, 2009).

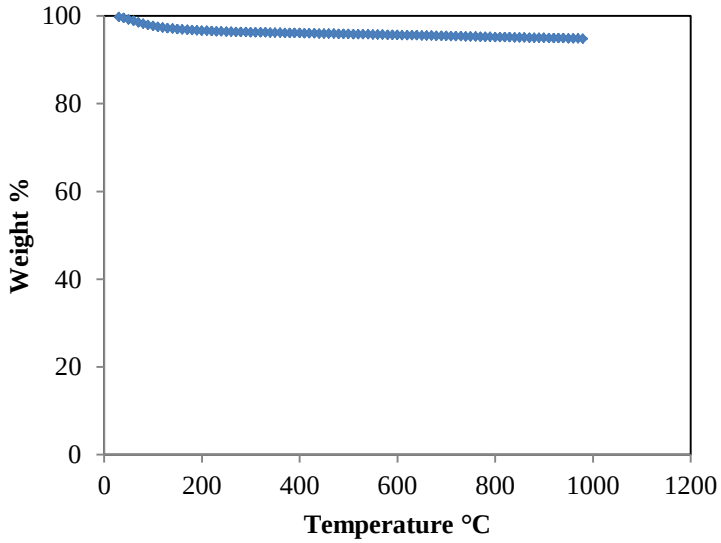

Figure 5.13 TGA profile for 20% MnO_x/Ce-γAl_2O_3

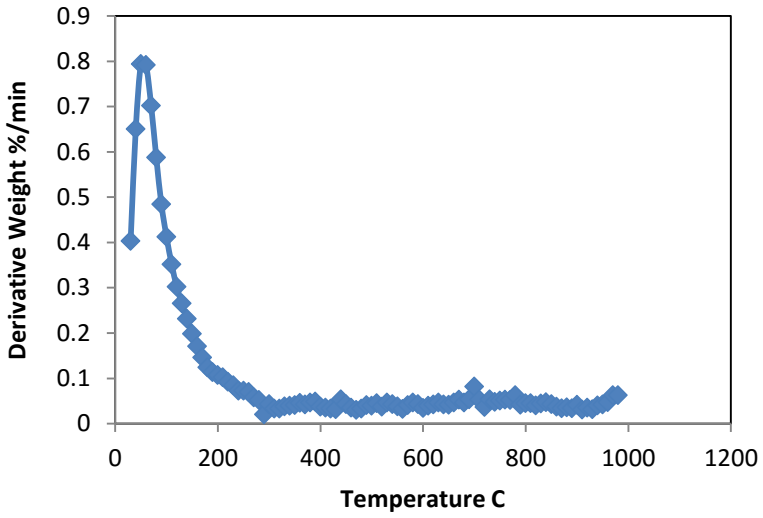

Figure 5.14 Derivative weight profile for 20% MnO_x/Ce-γAl_2O_3

5.3. Liquid fuel CLC in fluidized CREC Riser Simulator

The reactivity of the prepared manganese oxide supported over gamma alumina was carried in the Riser reactor. The combustion reaction was carried out at different temperatures and atmospheric pressure. Complete re-oxidation of the reduced oxygen carrier was achieved in air flow for 10 minutes.

Figure 5.15 shows a pressure profile for the vacuum box and the reactor during the combustion reaction. The lower curve in Figure 5.15 represents the pressure profile in the vacuum box, which remained constant during the reaction period. At termination time, the reactor pressure is decreased while the vacuum box pressure is slightly increased with these pressure changes.

The gaseous products contained in the Riser Reactor vacuum box were analyzed using two detectors. Flame Ionization detector (FID) was used to analyze the organic hydrocarbons while thermal conductivity detector (TCD) was used for CO and CO_2. Figure 5.16 shows a sample chromatogram of the gaseous products after a reaction run.

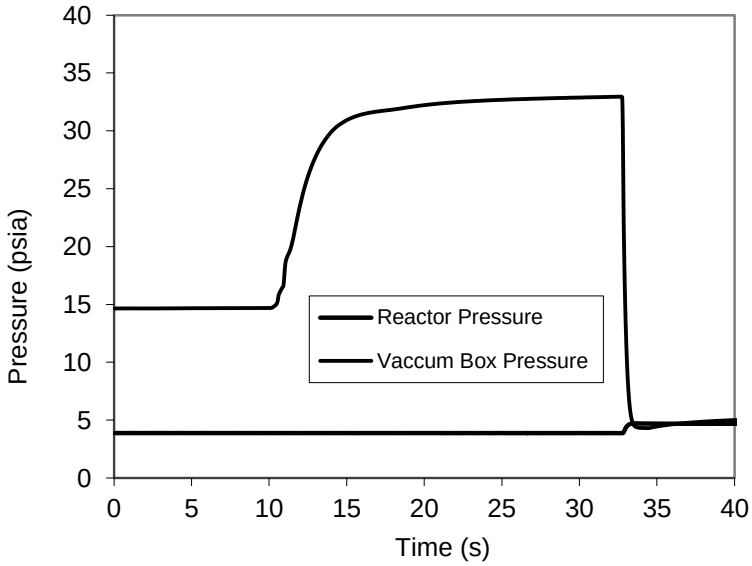

Figure 5.15 A typical pressure profile for the reactor and vacuum box during a CLC run (T: 475 °C; P: 1 atm; contact time: 20 sec;Wcarrier: 0.7 g)

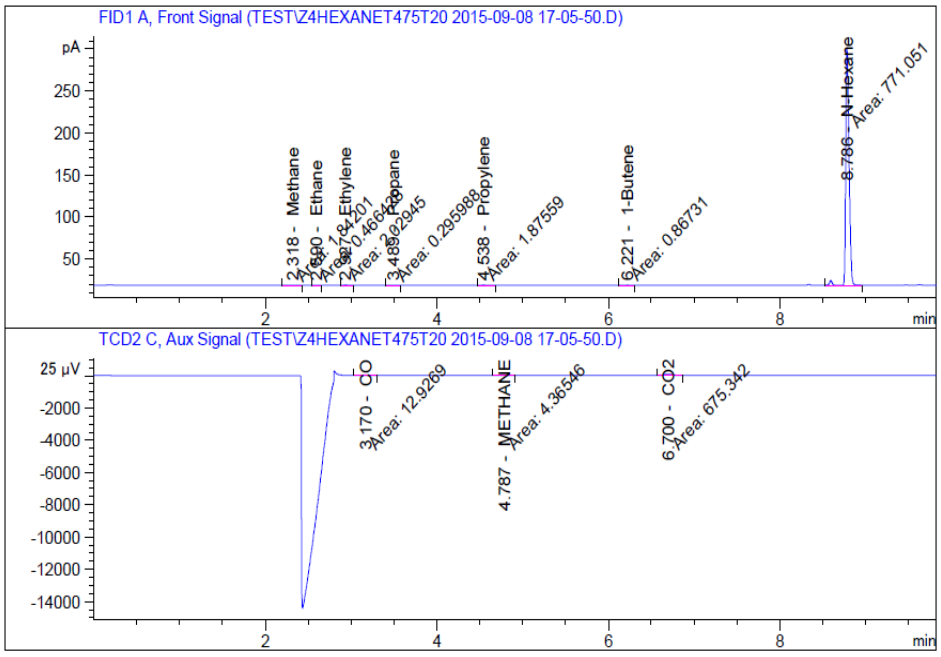

Figure 5.16 Gas Chromatographic analysis of gaseous products for hexane CLC in the CREC Riser Simulator after a CLC run (T: 475 °C; P: 1 atm; contact time:20 sec; Wcarrier: 0.7 g).

The CLC hexane experiments were conducted under fluidized bed conditions. All the experiments were carried out using same feed to oxygen carrier ratios. After each run, the product gas was analyzed by a GC. Following each CLC run, the oxygen carrier was regenerated by circulating air through the fluidized oxygen carrier bed. Table 5.4 reports the products distribution of the hexane CLC experiments over MnOx/ Ce-γ-Al2O3 oxygen carrier at various temperature levels.

Table5.4 Products distribution of the hexane CLC experiments over MnOx/ Ce-γ-Al2O3 oxygen carrier at various temperature levels (P: 1 atm; contact time: 20 sec; W: 0.7 g).

Temp (C^0)	mole fraction distribution results of Hexane CLC experiments				
	CO_2	CO	C_6H_{14}	CH_4	other HC
500	0.404	0.009	0.564	0.005	0.017
525	0.453	0.022	0.447	0.008	0.070
550	0.541	0.227	0.186	0.037	0.010
575	0.472	0.291	0.094	0.129	0.014
600	0.467	0.285	0.093	0.123	0.032
625	0.469	0.276	0.077	0.153	0.025
650	0.551	0.239	0.059	0.130	0.021

The GC data were further processed to calculate conversion and selectivity of various products using the following definitions:

$$\text{Conversion of Hexane} = \frac{\text{moles of hexane converted}}{\text{moles of hexane fed}}$$

$$\text{Selectivity of product i} = \frac{\text{moles of product i}}{\text{total products moles} - \text{moles of product i}}$$

Figure 5.17 shows the influence of temperature on the hexane conversion and the main products selectivity using 20% MnO_x/Al_2O_3 oxygen carrier. At low reaction temperature, the low conversion is mainly due to minimum availability of the reducible oxygen as revealed in TPR study. As shown in Figure 5.17, as the reaction temperature increases, hexane conversion increases to 55.34 %, 81.45% and 90.77% at 550 ^{o}C. On the other hand, CO_2 selectivity showed a gradual decrease with increasing reaction temperature. This trend is expected due to the exothermic nature of the reaction between manganese oxide and hexane. Moreover, Figure 5.17 shows that the increase in hexane conversion and the decrease in CO_2 selectivity with reaction temperature are accompanied by an increase in the selectivity to CO. Also, From the GC results, there is a formation of CH_4 with increasing trend as the temperature increases.

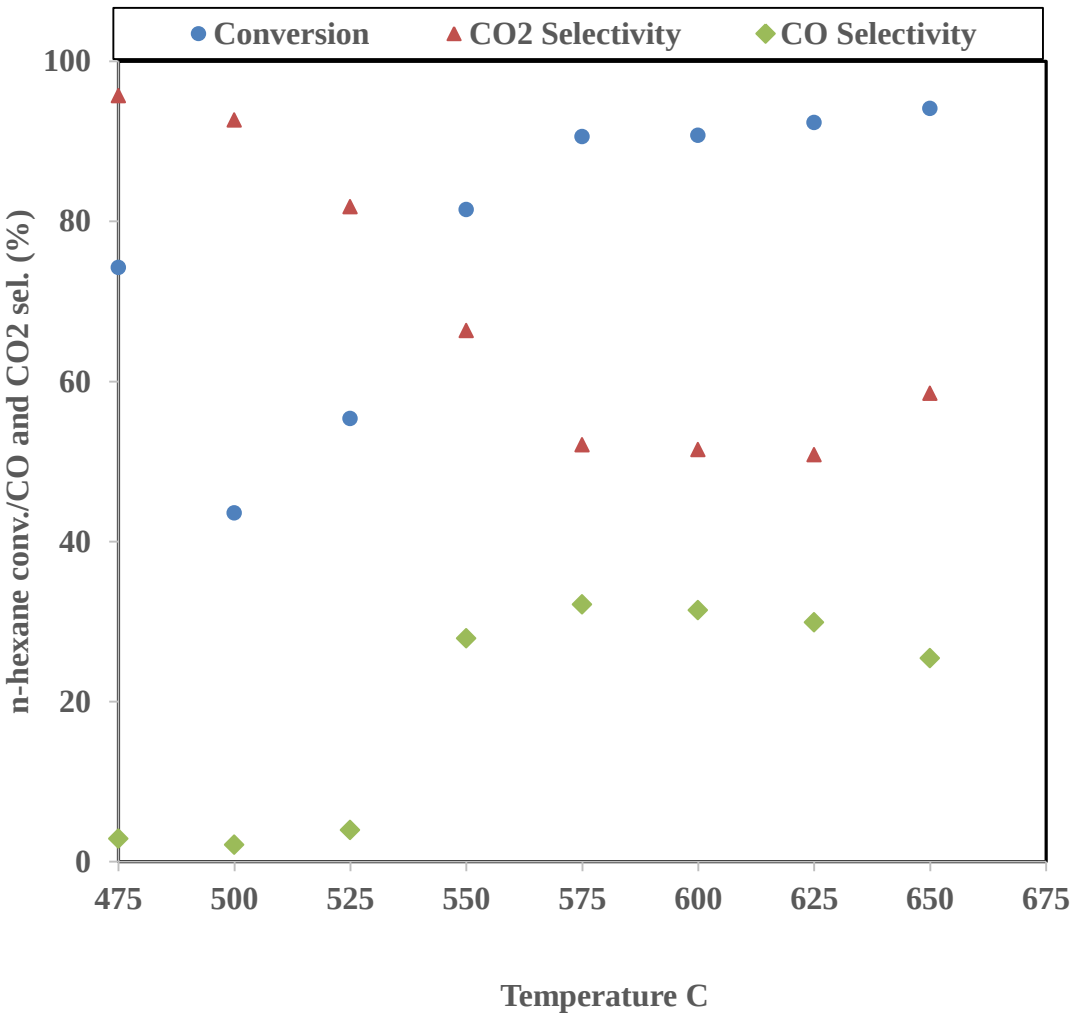

Figure 5.17 Effect of temperature on n-hexane conversion, CO_2 and CO selectivity 20% MnO_x/Ce-γAl_2O_3 (P: 1 atm; contact time: 20 sec; W: 0.7 g).

The following reactions can be proposed to explain the hexane combustion results in the Riser Simulator:

$$C_mH_n + m\,MO_x \rightarrow m\,CO + \frac{n}{2}\,H_2 + m\,MO_{x-1} \quad \text{(R1)}$$

$$C_mH_n + m\,H_2O \rightarrow m\,CO + \left(\frac{n}{2} + m\right)H_2 \quad \text{(R2)}$$

$$CO + MO_x \rightarrow CO_2 + MO_{x-1} \quad \text{(R3)}$$

$$H_2 + MO_x \rightarrow MO_{x-1} + H_2 \quad \text{(R4)}$$

$$CO + H_2O \rightarrow CO_2 + H_2 \quad \text{(R5)}$$

The major products of n-hexane CLC experiments were H_2, CH_4, CO and CO_2. CH_4 is an intermediate product resulting from thermal cracking of hexane. This interprets the increasing trend in the formation of CH_4 as the temperature increases. Also, H_2 and CO are intermediate products from hexane combustion in the CLC process. H_2 and CO could be formed from partial oxidation (R1) or steam reforming (R2).

The complete combustion of these intermediate is represented by (R3) and (R4). Also, the water gas shift reaction (R5) converts the CO intermediate to CO_2 and H_2. At high temperature, the intermediate products are favorable while CO_2 is favorable at low temperature. This explains the temperature effect on the product distribution, as seen in Figure 5.17.

Figure 5.18 shows the influence of contact time on the hexane conversion and the main products selectivity using 20% MnO_x/Al_2O_3 oxygen carrier and 550 ℃. As expected, as the reaction time increases, hexane conversion increases to 91.77% at 20 ℃. On the other hand, CO_2 selectivity showed a gradual decrease with increasing reaction temperature. Moreover, the CO selectivity was increased with increasing the contact time. This is could be explain by the catalytic effect of metal manganese as the contact time increased.

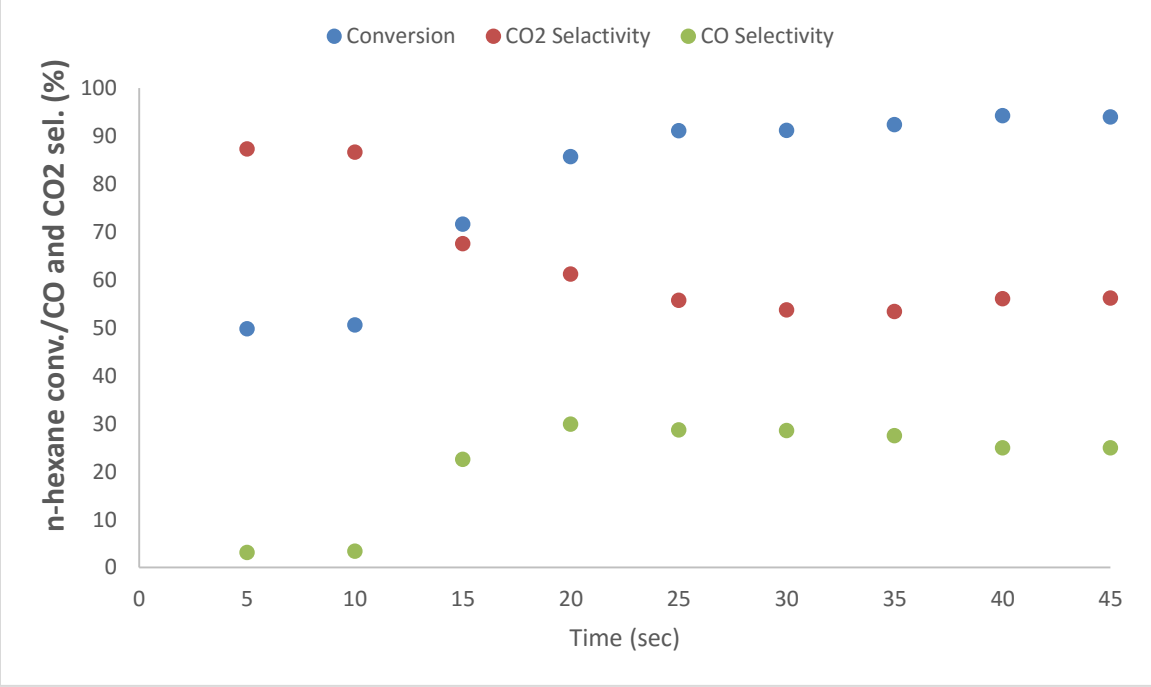

Figure 5.18 Effect of contact time on n-hexane conversion, CO2 and CO selectivity 20% MnOx/Ce-γAl2O3 (P: 1 atm; T: 550 ℃; W: 0.7 g).

Also, the oxygen carrier sample was analyzed for total organic carbon using TOC analyzer. The result showed that only limited amount (555.23 micro gram of carbon per gram sample) of coke was formed. This is an important result since coke formation lead to decrease the CO_2 capture efficiency.

5.4. Solid Gas Reaction kinetics

TPR kinetics can be formulated considering an overall reaction rate being a function of the solid material reduction $f(\alpha)$ and the compositions of the gas phase. The function of the degree of conversion $f(\alpha)$ depends on the model applied in the determination of the kinetics (Kanervo & Krause, 2001).

$$\frac{d\alpha}{dt} = k(T)f(\alpha)f(p_A, p_B)$$

where, α is degree of reduction, k (t) is reaction constant and $f(P_A, P_B)$ are reactant and product partial pressures. The degree of reduction (α) during the solid-state reaction can be written as:

$$\alpha(t) = \frac{\Delta n_t}{\Delta n_{total}}$$

Where, nt is the moles of H_2 consumed at time t (min), Δn_{total} is the total moles of H_2 consumed it the whole reduction or oxidation cycle. The function $f(P_A, P_B)$ can be considered as constant as all the TPR experiments were carried out at same feed flow rate, hydrogen partial pressure resulting to the following equation:

$$\frac{d\alpha}{dt} = k(T)f(\alpha)$$

Were the rate constant is expressed by Arrhenius equation:

$$k = k_0 \exp\left[\frac{-E_{app}}{R}\left(\frac{1}{T} - \frac{1}{T_m}\right)\right]$$

where, E_{app} is the activation energy, k_0 is the pre-exponential factor and Tm the centering temperature to minimize cross correlation between parameters.

During TPR, then temperature increases linearly as follows:

$T = T_0 + \beta$ And it follows that

$$\frac{dT}{dt} = \beta$$

And, since

$$\left(\frac{d\alpha}{dt}\right) = \left(\frac{d\alpha}{dT}\right)\left(\frac{dT}{dt}\right) = \beta\left(\frac{d\alpha}{dT}\right)$$

Avrami nucleation and growth model will be used in this model. The function of the degree of reduction $f(\alpha)$ for the nucleation and growth model is given by:

$$f(\alpha) = n(1-\alpha)[-\ln(1-\alpha)]^{(n-1)/n}$$

where, n is the Avrami exponent indicative of the reaction mechanism and crystal growth dimension. n equals one leads to random nucleation, two leads to a 2-dimensional nuclei growth and three 3-dimensinoal nuclei growth (Kanervo & Krause, 2001). The final model equation cab be written as:

$$\left(\frac{d\alpha}{dT}\right) = -\frac{k_0}{\beta} n(1-\alpha)[-\ln(1-\alpha)]^{\frac{n-1}{n}} \; Exp\left(-\frac{E}{R}\left(\frac{1}{T} - \frac{1}{T_m}\right)\right)$$

Table 5.5 Estimated kinetic parameters of Avrarmi- Erofyev

Experiment	Fuel	E (KJ/mole)	R2
TPR	H2	26.9	0.995
Riser Simulator	C6H14	59.2	0.966

Using Mathematica, Regression was achieved using TPR data. Figure. 5.19 shows the model predicted versus the experimental a (degree of reduction) using Avarmi–Erofeyev model.

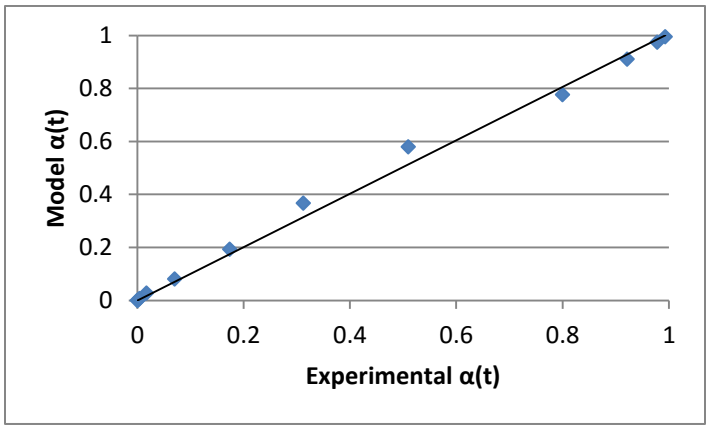

Figure 5.19 Experimental and predicted $\alpha(t)$ of TPR data.

Also, the Avrami-Erfeyev model was used to fit the experimental data for the Riser Simulator. Figure 5.20 displays a comparison between nucleation model and the Riser data. A good regression results were obtained with n =1. Thus, a random nucleation model represents reduction of the supported manganese oxide, which is an indication of the very limited crystallite growth. The estimated kinetic parameters and the corresponding R^2 are shown presented in Table 5.5. All these statistical indicators favorably indicate the goodness of the model fitting. Also, The combined experimental and predicted results for $\alpha(t)$ is shown in Figure 5.21.

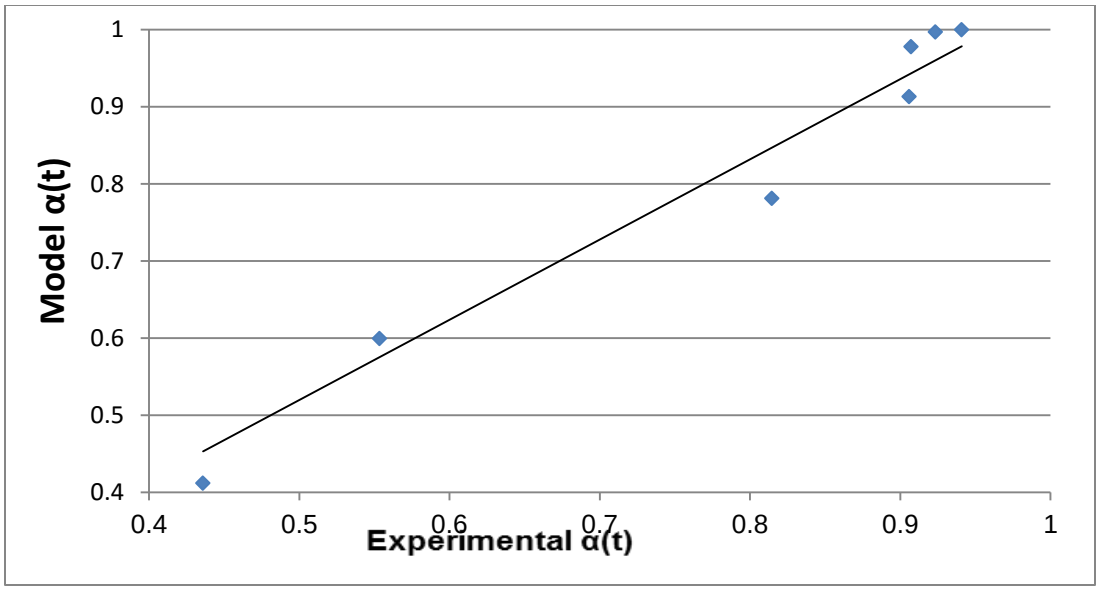

Figure 5.20 Experimental and predicted α(t) of Riser Simulator data.

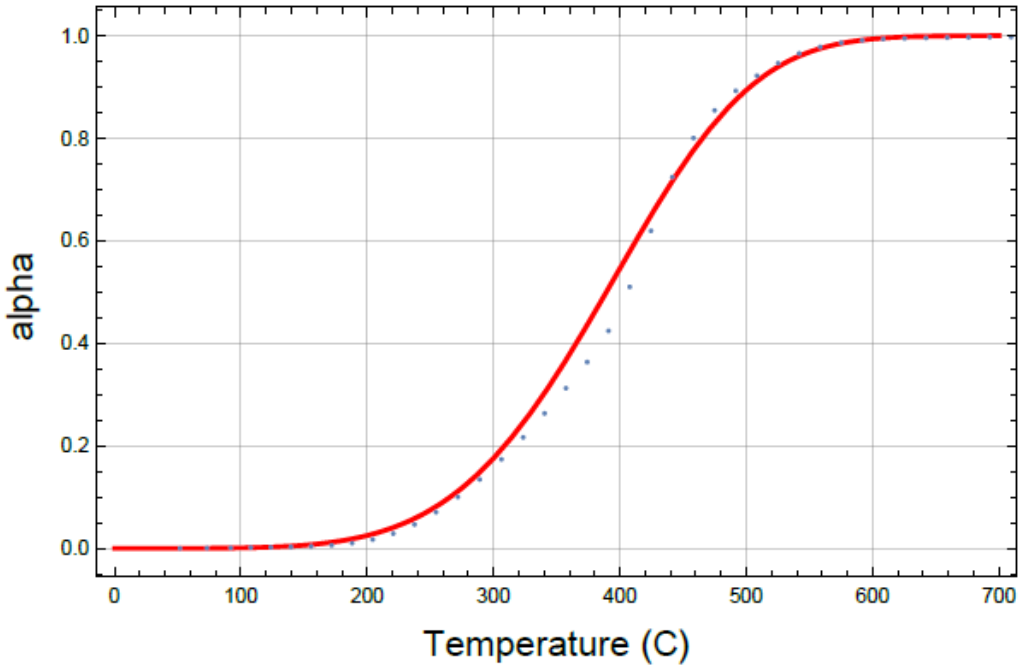

Figure 5.21 Experimental and Predicted results of the degree of reduction

CHAPTER 6

CONCLUSION AND RECOMMENDATIONS

In this study, Ce modified MnO_x/Ce-γAl_2O_3 oxygen carriers were synthesized, characterized and evaluated in a fluidized CREC Riser Simulator using n-hexane as liquid fuel. Following are the conclusion of this investigation:

1- Ce modification improves the thermal stability of gamma alumina and hinders the formation of difficult reducing manganese aluminate.
2- XRD of fresh MnO_x/Ce-γAl_2O_3 shows only Mn_2O_3 and γAl_2O_3 phases.
3- TGA and BET surface area analysis confirms the stability of the prepared oxygen carriers by maintaining the surface area of the samples.
4- TPR result shows excellent reduction performance MnO_x/Ce-γAl_2O_3 oxygen carriers. Almost 83% of the loaded MnO_x are reduced over the repeated TPR/TPO cycles.
5- NH_3-TPD analysis shows that 15 %MnO_x/Ce-γAl_2O_3 has lower acidity that that of 20 % MnO_x/Ce-γAl_2O_3 sample.
6- The analysis of the reduction gases products obtained in the CREC Riser Simulator showed that 15 Mn is more reactive than 20 Mn.
7- The Avrami model (with n=1) is found to describe the TPR data adequately.
8- The CLC cycles using n-hexane as liquid fuel shows that CO_2 is the main combustion products and 90 % hexane combustion can be achieved at 575 °C

which is consistent to the reduction data of the prepared oxygen carrier.

9- The solid state kinetics indicate that a nucleation and nuclei growth model adequately describe the reduction profile of the MnO_x/Ce-γAl_2O_3 oxygen carrier. The estimated activation energy is found to be 27 kJ/mole which is similar to what is reported in the literature.

Also, the following works are recommended:

i. Thermal runs for hexane in order to investigate the mechanism of reactions.
ii. Preparation and evaluation of bimetallic manganese based oxygen carriers such as Mn-Fe and Mn-Cu.
iii. Synthesis of oxygen carriers using different methods to optimize the performance of the prepared oxygen carriers.

REFERENCE

Abad, A., Mattisson, T., Lyngfelt, A., & Rydén, M. (2006). Chemical-looping combustion in a 300W continuously operating reactor system using a manganese-based oxygen carrier. *Fuel*, *85*(9), 1174–1185.

Adanez, J., de Diego, L. F., Garcia-Labiano, F., Gayán, P., Abad, A., & Palacios, J. M. (2004). Selection of oxygen carriers for chemical-looping combustion [32]. *Energy & Fuels*, *18*(2), 371–377.

Álvarez-Galván, M. C., de la Peña O'Shea, V. A., Fierro, J. L. G., & Arias, P. L. (2003a). Alumina-supported manganese- and manganese–palladium oxide catalysts for VOCs combustion. *Catalysis Communications*, *4*(5), 223–228. http://doi.org/10.1016/S1566-7367(03)00037-2

Álvarez-Galván, M. C., de la Peña O'Shea, V. A., Fierro, J. L. G., & Arias, P. L. (2003b). Alumina-supported manganese- and manganese–palladium oxide catalysts for VOCs combustion. *Catalysis Communications*, *4*(5), 223–228. http://doi.org/10.1016/S1566-7367(03)00037-2

Álvarez-Galván, M. C., Pawelec, B., de la Peña O'Shea, V. A., Fierro, J. L. G., & Arias, P. L. (2004). Formaldehyde/methanol combustion on alumina-supported manganese-palladium oxide catalyst. *Applied Catalysis B: Environmental*, *51*(2), 83–91. http://doi.org/10.1016/j.apcatb.2004.01.024

Anna Galiková, A. G. (n.d.). The global approach to TPD and isothermal adsorption - desorption kinetics.

Brandvoll, O., & Bolland, O. (2004). Inherent CO2 Capture Using Chemical Looping Combustion in a Natural Gas Fired Power Cycle. *Journal of Engineering for Gas Turbines and Power*, *126*(2), 316–321. http://doi.org/10.1115/1.1615251

Cavani, F., & Trifiró, F. (1997). Classification of industrial catalysts and catalysis for the petrochemical industry. *Catalysis Today*, *34*(3–4), 269–279. http://doi.org/10.1016/S0920-5861(96)00054-5

Chester, A. W., & Derouane, E. G. (2009). *Zeolite Characterization and Catalysis: A Tutorial*. Springer Science & Business Media.

Cho, P., Mattisson, T., & Lyngfelt, A. (2004). Comparison of iron-, nickel-, copper- and manganese-based oxygen carriers for chemical-looping combustion. *Fuel*, *83*(9), 1215–1225. http://doi.org/10.1016/j.fuel.2003.11.013

Cui, D., Liu, J., Yu, J., Yue, J., Su, F., & Xu, G. (2015). Necessity of moderate metal-support interaction in Ni/Al $_2$ O $_3$ for syngas methanation at high temperatures. *RSC Adv.*, *5*(14), 10187–10196. http://doi.org/10.1039/C4RA14652B

Dennis, J. S., Scott, S. A., & Hayhurst, A. N. (2006). In situ gasification of coal using steam with chemical looping: a technique for isolating CO2 from burning a solid fuel. *Journal of the Energy Institute*, *79*(3), 187–190.

Edenhofer, O., Pichs-Madruga, R., Sokona, Y., Seyboth, K., Kadner, S., Zwickel, T., … Matschoss, P. (2011). *Renewable Energy Sources and Climate Change Mitigation: Special Report of the Intergovernmental Panel on Climate Change*. Cambridge University Press.

Fang, H., Haibin, L., & Zengli, Z. (2009). Advancements in Development of Chemical-Looping Combustion: A Review. *International Journal of Chemical Engineering*,

2009, e710515. http://doi.org/10.1155/2009/710515

Forret, A., Hoteit, A., & Gauthier, T. (2009). Chemical Looping Combustion Process applied to liquid fuels. *British–French Flame Days, Lille, France*, 37–37.

HORST J. RICHTER, & KARL F. KNOCHE. (1983). Reversibility of Combustion Processes. In *Efficiency and Costing* (Vol. 235, pp. 71–85). AMERICAN CHEMICAL SOCIETY. Retrieved from http://dx.doi.org/10.1021/bk-1983-0235.ch003

Hossain, M. M., & de Lasa, H. I. (2008). Chemical-looping combustion (CLC) for inherent separations—a review. *Chemical Engineering Science*, *63*(18), 4433–4451. http://doi.org/10.1016/j.ces.2008.05.028

Hu, J., Chu, W., & Shi, L. (2008). Effects of carrier and Mn loading on supported manganese oxide catalysts for catalytic combustion of methane. *Journal of Natural Gas Chemistry*, *17*(2), 159–164. http://doi.org/10.1016/S1003-9953(08)60044-4

Ishida, M., Jin, H., & Okamoto, T. (1996). A Fundamental Study of a New Kind of Medium Material for Chemical-Looping Combustion. *Energy & Fuels*, *10*(4), 958–963. http://doi.org/10.1021/ef950173n

Ishida, M., Jin, H., & Okamoto, T. (1998). Kinetic behavior of solid particle in chemical-looping combustion: suppressing carbon deposition in reduction. *Energy & Fuels*, *12*(2), 223–229.

Jenni, K. E., Baker, E. D., & Nemet, G. F. (2013). Expert elicitations of energy penalties for carbon capture technologies. *International Journal of Greenhouse Gas Control*, *12*, 136–145. http://doi.org/10.1016/j.ijggc.2012.11.022

Jerndal, E., Mattisson, T., & Lyngfelt, A. (2006a). Thermal Analysis of Chemical-Looping Combustion. *Chemical Engineering Research and Design*, *84*(9), 795–806. http://doi.org/10.1205/cherd05020

Jerndal, E., Mattisson, T., & Lyngfelt, A. (2006b). Thermal Analysis of Chemical-Looping Combustion. *Chemical Engineering Research and Design*, *84*(9), 795–806. http://doi.org/10.1205/cherd05020

Johansson, M., Mattisson, T., & Lyngfelt, A. (2006). Comparison of oxygen carriers for chemical-looping combustion [172]. *Thermal Science*, *10*(3), 93–107.

Johansson, M., Mattisson, T., & Lyngfelt, A. (2006). Investigation of Mn3O4 With Stabilized ZrO2 for Chemical-Looping Combustion. *Chemical Engineering Research and Design*, *84*(9), 807–818. http://doi.org/10.1205/cherd.05206

Jones, D., Bhattacharyya, D., Turton, R., & Zitney, S. E. (2011). Optimal design and integration of an air separation unit (ASU) for an integrated gasification combined cycle (IGCC) power plant with CO2 capture. *Fuel Processing Technology*, *92*(9), 1685–1695. http://doi.org/10.1016/j.fuproc.2011.04.018

Kanervo, J. M., & Krause, A. O. I. (2001). Kinetic Analysis of Temperature-Programmed Reduction: Behavior of a CrOx/Al2O3 Catalyst. *The Journal of Physical Chemistry B*, *105*(40), 9778–9784. http://doi.org/10.1021/jp0114079

Kemp, R. B. (1999). *Handbook of Thermal Analysis and Calorimetry: From Macromolecules to Man* (Vol. 4). Elsevier. Retrieved from http://books.google.com/books?hl=ar&lr=&id=sqZ2p9AzKNIC&oi=fnd&pg=PP2&dq=Comprehensive+Handbook+of+Calorimetry+and+Thermal+Analysis..&ots=XJz4RdkZzp&sig=A1GUMMIN_hvmdj8LxjTdy_Qkdeg

Kokes, R. J., Tobin Jr, H., & Emmett, P. H. (1955). New microcatalytic-chromatographic technique for studying catalytic reactions. *Journal of the American Chemical Society*, *77*(22), 5860–5862.

Leion, H., Mattisson, T., & Lyngfelt, A. (2007). The use of petroleum coke as fuel in chemical-looping combustion. *Fuel*, *86*(12), 1947–1958.

Liu, F., Zhang, Y., Chen, L., Qian, D., Neathery, J. K., Kozo, S., & Liu, K. (2013). Investigation of a Canadian Ilmenite as an Oxygen Carrier for Chemical Looping Combustion. *Energy & Fuels*, *27*(10), 5987–5995. http://doi.org/10.1021/ef401513p

Lyngfelt, A., Leckner, B., & Mattisson, T. (2001). A fluidized-bed combustion process with inherent CO2 separation; application of chemical-looping combustion. *Chemical Engineering Science*, *56*(10), 3101–3113. http://doi.org/10.1016/S0009-2509(01)00007-0

Lyngfelt, A., & Thunman, H. (2005). Construction and 100 h of operational experience of a 10-kW chemical-looping combustor. *Carbon Dioxide Capture for Storage in Deep Geologic Formations; Results from the CO2 Capture Project*, *1*, 625–645.

Mathias, P. M., Reddy, S., Smith, A., & Afshar, K. (2013). Thermodynamic analysis of CO2 capture solvents. *International Journal of Greenhouse Gas Control*, *19*, 262–270. http://doi.org/10.1016/j.ijggc.2013.09.001

Mattisson, T., Järdnäs, A., & Lyngfelt, A. (2003). Reactivity of Some Metal Oxides Supported on Alumina with Alternating Methane and OxygenApplication for Chemical-Looping Combustion. *Energy & Fuels*, *17*(3), 643–651. http://doi.org/10.1021/ef020151i

Mattisson, T., Lyngfelt, A., & Leion, H. (2009). Chemical-looping with oxygen uncoupling for combustion of solid fuels. *International Journal of Greenhouse Gas Control*, *3*(1), 11–19. http://doi.org/10.1016/j.ijggc.2008.06.002

Moldenhauer, P., Rydén, M., Mattisson, T., Hoteit, A., Jamal, A., & Lyngfelt, A. (2014). Chemical-Looping Combustion with Fuel Oil in a 10 kW Pilot Plant. *Energy & Fuels*, *28*(9), 5978–5987. http://doi.org/10.1021/ef5014677

Moldenhauer, P., Rydén, M., Mattisson, T., & Lyngfelt, A. (2012). Chemical-looping combustion and chemical-looping with oxygen uncoupling of kerosene with Mn- and Cu-based oxygen carriers in a circulating fluidized-bed 300 W laboratory reactor. *Fuel Processing Technology*, *104*, 378–389. http://doi.org/10.1016/j.fuproc.2012.06.013

Neurock, M. (1994). The microkinetics of heterogeneous catalysis. By J. A. Dumesic, D. F. Rudd, L. M. Aparicio, J. E. Rekoske, and A. A. Treviño, ACS Professional Reference Book, American Chemical Society, Washington, DC, 1993, 315 pp. *AIChE Journal*, *40*(6), 1085–1087. http://doi.org/10.1002/aic.690400620

Ortiz, M., de Diego, L. F., Gayán, P., Pans, M. A., García-Labiano, F., Abad, A., & Adánez, J. (2010). Hydrogen production coupled with CO2 capture by chemical-looping using mixed Fe-Ni oxygen carriers. In *Proc. 1st Int Conf on Chemical Looping. Lyon, France*.

Ozawa, M., & Kimura, M. (1990). Effect of cerium addition on the thermal stability of gamma alumina support. *Journal of Materials Science Letters*, *9*(3), 291–293. http://doi.org/10.1007/BF00725828

Padurean, A., Cormos, C.-C., & Agachi, P.-S. (2012). Pre-combustion carbon dioxide

capture by gas–liquid absorption for Integrated Gasification Combined Cycle power plants. *International Journal of Greenhouse Gas Control*, *7*, 1–11. http://doi.org/10.1016/j.ijggc.2011.12.007

Peluso, M. A., Pronsato, E., Sambeth, J. E., Thomas, H. J., & Busca, G. (2008). Catalytic combustion of ethanol on pure and alumina supported K-Mn oxides: An IR and flow reactor study. *Applied Catalysis B: Environmental*, *78*(1–2), 73–79. http://doi.org/10.1016/j.apcatb.2007.09.002

Perrichon, V., Retailleau, L., Bazin, P., Daturi, M., & Lavalley, J. C. (2004). Metal dispersion of CeO2–ZrO2 supported platinum catalysts measured by H2 or CO chemisorption. *Applied Catalysis A: General*, *260*(1), 1–8. http://doi.org/10.1016/j.apcata.2003.09.031

Pimenidou, P., Rickett, G., Dupont, V., & Twigg, M. V. (2010). Chemical looping reforming of waste cooking oil in packed bed reactor. *Bioresource Technology*, *101*(16), 6389–6397.

Rydén, M., Moldenhauer, P., Mattisson, T., Lyngfelt, A., Younes, M., Niass, T., … Ballaguet, J.-P. (2013). Chemical-Looping Combustion with Liquid Fuels. *Energy Procedia*, *37*, 654–661. http://doi.org/10.1016/j.egypro.2013.05.153

Singleton, A. H., & Oukaci, R. (2001, July 3). Highly active Fischer-Tropsch synthesis using doped, thermally stable catalyst support. Retrieved from http://www.google.com.ar/patents/US6255358

Siriwardane, R., Tian, H., Richards, G., Simonyi, T., & Poston, J. (2009). Chemical-looping combustion of coal with metal oxide oxygen carriers [227]. *Energy & Fuels*, *23*(8), 3885–3892.

Stobbe, E. R., De Boer, B. A., & Geus, J. W. (1999). The reduction and oxidation behaviour of manganese oxides [242]. *Catalysis Today*, *47*(1), 161–167.

Stock, S. R., & Cullity, B. D. (2001). Elements of X-ray diffraction. *Prentice Hall, New Jersey, 2001) P*, *275*. Retrieved from http://citeadi.phpnet.us/r/elements-of-x-ray-diffraction-by-s-r-stock.pdf

Tian, H., Simonyi, T., Poston, J., & Siriwardane, R. (2009). Effect of hydrogen sulfide on chemical looping combustion of coal-derived synthesis gas over bentonite-supported metal- oxide oxygen carriers [226]. *Industrial & Engineering Chemistry Research*, *48*(18), 8418–8430.

US Department of Commerce, N. (2014). ESRL Global Monitoring Division - Global Greenhouse Gas Reference Network. Retrieved November 16, 2014, from http://www.esrl.noaa.gov/gmd/ccgg/trends/

US Department of Energy, Carbon Dioxide Capture and Storage. (n.d.). Retrieved March 28, 2015, from https://www.google.com/search?q=US+Department+of+Energy,+N.+DOE/NETL+Carbon+Dioxide+Capture+and+Storage+RD%26D+Roadmap%3B+2010&hl=ar&authuser=0#hl=ar&authuser=0&q=US+Department+of+Energy%2C+Carbon+Dioxide+Capture+and+Storage+RD%26D+Roadmap%3B+2010

Wallin, E., Andersson, J. M., Chirita, V., & Helmersson, U. (2004). Effects of additives in α- and θ-alumina: an ab initio study. *Journal of Physics: Condensed Matter*, *16*(49), 8971. http://doi.org/10.1088/0953-8984/16/49/012

Yu, H. (2013). Carbon Capture and Storage: A Challenging Approach for Mitigation of Global Warming. *International Journal of Clean Coal and Energy*, *02*(03), 23–24.

VITAE

Name :Abdulhadi Abdullah Hassan Al-Omari Al-Zahrani

Nationality :Saudi

Date of Birth :10/27/1989

Email :aahadi703@gmail.com

Address :Dhahran, Saudi Arabia

Academic Background:

- B.Sc. degree in Chemical Engineering King Fahd University of Petroleum and Minerals, Dhahran, Saudi Arabia (2012).
- M.Sc. degree in Chemical Engineering King Fahd University of Petroleum and Minerals Dhahran, Saudi Arabia (2015).